

Control Design for an Inertially Stabilized Rifle

Alejandro Porter White

Thesis submitted to the faculty of the
Virginia Polytechnic Institute and State University
in partial fulfillment of the requirements
for the degree of

Master of Science

in

Electrical Engineering

Dr. Douglas K. Lindner, Chairman
Dept. of Electrical Engineering

Dr. William T. Baumann
Dept. of Electrical Engineering

Dr. Wayne A. Scales
Dept. of Electrical Engineering

December 12, 2007
Blacksburg, Virginia

Keywords: Jitter, Active Stabilization, INSTAR, Disturbance Rejection, Control

Control Design for an Inertially Stabilized Rifle

Alejandro Porter White

Abstract

An alternate method for mitigating the depredateing physiological affects of a soldiers marksmanship due to combat stressors can be achieved through the design and implementation of a active stabilization system for small arms weapons. The INSTAR system is an innovative active stabilization system designed to decouple the shooter's disturbance effects from the barrel movement. The INSTAR system uses an piezoelectric actuator separating the barrel of the rifle from its stock to stabilize barrel movement. This paper uses various control techniques to develop control algorithms for simulation. The level of performance for each control algorithm is based on how well each they measure up to the criteria developed from the INSTAR. This paper furthers research on INSTAR by developing and comparing four control designs that may be implemented within the INSTAR system.

Acknowledgements

I would like to thank my advisor Dr. Douglas Lindner, for his uncompromising support. Who stuck with me through my entire graduate school experience, not just for my thesis. I would also like to thank my family and friends for the resources and support that they provided during my time here in graduate. Last but not least I want to acknowledge the person who gave me the will to keep going at times that I would have normally quit, my wonderful son, Joseph. Thank you all.

Contents

Chapter 1: Introduction	1
1.1 Physiological Effects of Combat.....	2
1.2 Marksmanship Training.....	3
1.3 Negative Factors Impacting Training.....	3
1.4 Literature Review.....	4
1.5 M16.....	5
1.6 Closed Loop Controller.....	5
Chapter 2 Mathematical Model	8
2.1 Actuator.....	8
2.2 Model Description.....	11
2.3 M16 State Space.....	18
Chapter 3 Design Criteria	25
3.1 Constraints and Specifications.....	25
Chapter 4 Control Techniques	28
4.1 Unity Feedback Gain.....	28
4.2 Compensator.....	30
4.3 State Feedback Matrix Gain.....	39
4.4 Observer Design.....	46
4.5 LQG.....	52
Chapter 5 Numerical Models	56
5.1 Uncontrolled System.....	56

5.2 Unity Feedback.....	58
5.3 Compensator Design.....	60
5.4 State Feedback Matrix.....	63
5.5 Observer Design.....	68
5.6 Linear Quadratic Gaussian.....	73
Chapter 6 Results	76
6.1 Uncontrolled System.....	76
6.2 Unity Feedback.....	78
6.3 Compensator.....	81
6.4 State Feedback.....	84
6.5 Observer.....	86
6.6 LQG.....	91
Chapter 7 Conclusion	95
References	98

List of Figures

2.1	Free Body Diagram Including Shoulder and Arm Disturbance	9
2.2	The Actuator's Piezoceramic Layers.....	9
2.3	Prototype Actuator for INSTAR.....	10
2.4	Allowable shooter targeting error range.....	10
2.5	Generic Dynamic Model with Active Stabilization.....	11
2.6	Dynamic M16 Combat Rifle Model with Active Stabilization.....	16
2.7	Block diagram of equation 2.29.....	23
3.1	Targeting Error Distribution.....	26
4.1	Negative Unity Feedback Control System.....	29
4.2	Control system w/negative unity feedback.....	31
4.3	Generic Root Locus with two Complex Poles.....	32
4.4	Generic Root Locus w/point p_e	34
4.5	Generic Root Locus w/180 degree departure angle.....	35
4.6	Possible K Values.....	36
4.7	Plant with state feedback matrix.....	40
4.8	Plant with observer connected to the state feedback matrix.....	47
4.9	LQG system with optimal feedback gain and optimal observer gain.....	55
5.1	Root locus of the uncontrolled system.....	57
5.2	Root locus of the plant connected to unity feedback system.....	59

5.3	Bode plot of the designed lead compensator's phase response.....	62
5.4	Root locus of the compensated original system.....	62
5.5	Root locus of the system with its poles placed by state feedback.....	67
5.6	Root locus of state feedback system with an observer.....	72
5.7	Root locus of LQG system.....	75
6.1	Targeting error for uncontrolled system.....	77
6.2	Actuator displacement of the uncontrolled system.....	78
6.3	Targeting error for uncontrolled system vs. unity feedback system.....	79
6.4	Actuator stabilization force of the unity feedback control system.....	80
6.5	Actuator displacement of the unity feedback control system.....	81
6.6	Targeting error for uncontrolled system vs. compensated system.....	82
6.7	Actuator stabilization force of the compensator control system.....	83
6.8	Actuator displacement of the compensator control system.....	83
6.9	Targeting error for uncontrolled system vs. state feedback system.....	84
6.10	Actuator stabilization force of the state feedback control system.....	85
6.11	Actuator displacement of the compensator control system.....	86
6.12	Targeting error for uncontrolled system vs. observer system.....	87
6.13	Actuator stabilization force of the observer control system.....	88
6.14	Actuator displacement of the observer control system.....	89
6.15	Actual state values vs. observer estimated state values.....	90
6.16	Targeting error for uncontrolled system vs. LQG control system.....	91
6.17	Actuator stabilization force of the LQG control system.....	92
6.18	Actuator displacement of the LQG control system.....	93

6.19 Actual state values vs. LQG estimated state values.....94

List of Tables

- 1.1 Marksmanship Skill Levels.....3
- 2.1 Actuator Specifications.....11
- 3.1 Maximum values of control constraints and specifications.....27
- 5.1 Open Loop Pole Location.....58
- 5.2 Open loop pole locations.....59
- 5.3 Open loop pole locations.....63
- 5.4 Desired pole locations placed by state feedback.....65
- 5.5 Actual pole locations place by state feedback.....68
- 5.6 Observer pole locations.....69
- 5.7 Pole locations of the state feedback with an observer.....73
- 5.8 Closed Loop Locations.....75

Chapter 1

Introduction

The security of the United States of America is defended daily by volunteer military personnel. The U.S. military is touted as the best in the world with the use of advanced technology, superior resources, and five service branches specializing in securing and protecting the land, air, and water. Despite these advantages, U.S. service members' lives are at risk every day as they attempt to defend our nation's interests. The number of military personnel in high risk combat situations grows each day. Over 200,000 active duty soldiers are currently serving in the war in Iraq, Operation Iraqi Freedom (DoD, Nov 2007). Since March 2003, the beginning of Operation Iraqi Freedom, more than 30,000 service members have been wounded (DoD, November 2007) and approximately 4,000 military personnel have died (DoD, November 2007). While government officials are trying to reduce soldier injuries and casualties by increasing funding, training, and number of military personnel, the figures continue to climb. Effective fighting tools borne of the application of today's latest technology are needed more than ever to maintain the U.S. strategic advantage and protect the U.S. soldier in any line of combat whether its on water, land, or in the air. This paper presents research to help protect and increase the defenses of infantry soldiers on ground. While in battle these soldiers' defenses and performance suffer due the intense stressors of combat.

1.1 Physiological Effects of Combat

Combat stress may be defined as the perception of an imminent threat of serious personal injury or death, or the stress of being tasked with the responsibility to protect another party from imminent and serious injury or death, under conditions where response time is minimal (cite). Physiological effects that result from combat include, but are not limited to, a dramatic increase in heart rate, heavy breathing, muscle tremors, and anxiety. Research shows that the heart rate of a soldier in combat is around 300 beats per minute (bpm), which is 100bpm more than the heart rate of Olympic athletes, which rarely exceed 200bpm during competition (Brei, James, Lindner, 2003). Fatigue is another physiological effect that is experienced by a soldier in combat. Depending on the soldier, the intensity of these physiological effects may render the soldier ineffective during combat.

The degradation of a soldier's marksmanship due to combat stressors is a problem that carries consequences and receives a great amount of attention from the United States military. Reduction in the soldier's accuracy leads to a decrease in the soldiers' ability to survive. A reduction in accuracy may also lead to an increase in collateral damage, as well as an increase in civilian casualties which in turn may have a negative impact on political relationships between the United States and other countries. Less accurate fire also results in an increased amount of wasted ammunition. The negative impact that combat stressors have on soldiers' marksmanship jeopardizes the missions, national security, and most importantly the lives of unit.

1.2 Marksmanship Training

Marksmanship is the measurement of a soldiers' rifle proficiency. It is a key component of successful missions and most importantly soldiers' defense. To reduce the physiological effects of combat, the U.S. military has developed extensive marksmanship training. This training includes physical and mental conditioning, along with rigorous target training exercises. One targeting exercise consists of soldiers shooting at pop-up targets at distances ranging from 50m-300m at various shooting positions (Brei et.al 2003). The skill levels for this exercise are shown in Table 1.1.

Table 1.1 Marksmanship Skill Levels

Expert	36 hits (minimum)
Sharpshooter	30 hits (minimum)
Marksman	23 hits (minimum)

In order for a soldier to advance to sniper training, they must qualify as an expert in this shooting exercise.

1.3 Negative Factors Impacting Training

Even though all soldiers receive marksmanship training, the number of soldiers that are able to qualify as Experts, is very low. This is due to that fact that it takes excellent motor skills and control over physiological effects which vary from soldier to soldier. Due to time constraints and urgent demands for soldier placement, marksmanship training for

incoming soldiers may be rushed. This creates a situation that is biased against those who have the potential to become Expert marksman if given the time normally allocated for training. Based on the intensity of stressors experienced by soldiers while in combat, it is well known that the accuracy of all shooters degrades during battle, regardless of the level of training.. An alternative solution to work in conjunction with marksmanship training, is to attach an active stabilization system to the small arms weapon of the soldiers. This system will act to increase the effectiveness of a soldiers' accuracy while experiencing the physiological effects of combat.

1.4 Literature Review

Statistics show that elimination of shooter induced disturbances can increase a soldier's accuracy by up to 25% (Brei et. al, 2003). This increase in accuracy may allow soldiers to qualify as an Expert marksman, who under normal circumstances would not. An increase in the number of Expert shooters will increase the soldiers' ability to defend themselves and increase mission effectiveness (Brei et. al, 2003). This is the motivation behind active stabilization systems. Active stabilization systems have been developed for large gun systems such as those on battleships, turreted systems like the 120mm gun on the M1A2 Abrams tanks, and the 30 mm gun on Apache Helicopters (Pathak, Brei, Luntz, Lavigne, 2006). However, research for the application of active stabilization systems on hand-held weapons is fairly new (Pathak et. al, 2006). The Inertially Stabilized Rifle (INSTAR) is an active stabilization system designed to remove user-induced disturbances in small arms weapon systems, particularly the M16 (Brei et. al 2003). The INSTAR system is designed to stabilize the barrel of the M16 through an active spring-damper system

placed between the barrel and stock of the M16 (Brei et. al 2003). A DC powered smart material actuator adjusts the elevation of the barrel to compensate for shooter induced disturbances forced upon the rifle through use of a closed loop feedback controller which is connected to gyroscopic sensors (Pathak et. al, 2006). The purpose of the feedback controller is to ensure that the active stabilization system operates at peak performance at all times.

1.5 M16

Since the 1960s the primary infantry rifle of the U.S. military has been the M16, 5.56-mm caliber, hand-held rifle. Today at least 15 NATO countries and 80 countries worldwide have used the M16 for defense. The M16 is the most commonly manufactured 5.56-mm rifle in the world. The United States and Canada have produced and distributed 8,000,000 M16s worldwide. It is estimated that 90% of these rifles are still in operation. In today's combat zones there is ever-increasing demand for a lightweight, highly dependable, accurate service rifle with great fire power. The M16 answers this call. Primarily composed of steel, aluminum, and composite plastics, most M16 rifles come in two forms: semi-automatic and 3 round burst. Both forms offer an effective range of 550m which is equivalent to 5.5 football field lengths (cite).

1.6 Closed Loop Controller

The INSTAR stabilization system is designed to save the lives of soldiers and those that they are sworn to protect. With this responsibility, it is imperative that the system

performs optimally at all times. The feedback controller is designed to use feedback received from the gyroscopic sensors to send commands that control the actuator's displacement of the gun barrel. This will offset the jitter like disturbances that are forced upon the rifle by a soldier in combat. The breathing pattern varies from soldier to soldier as well as how much each soldier is physiologically affected by combat. Therefore each soldier induces their own unique disturbances upon the rifle. A properly designed feedback controller will remove the shooter induced disturbances without over-exerting the actuator. It will send different commands to the actuator for disturbances of various intensities. For example, disturbances of different amplitudes and frequencies may not require the same amount of force exertion and amplitude displacement. By adapting to the different disturbances and sending control commands that are calculated to address to each disturbance, the feedback controller will prevent the actuator from using unnecessary energy on smaller disturbances. In turn, conserving battery life and conservation of battery life will provide the most "rounds fired" in combat per fully charged battery. This type of robust feedback controller will guarantee that the INSTAR system will perform correctly for all soldiers.

The following thesis presents just such a robust feedback controller. Chapter 2 shows the development of the mathematical model using the equations of motion for the M16 rifle. Chapter 3 outlines the specification and criteria that the control systems designed for the INSTAR system must meet. Chapter 4 consists of the theoretical underpinnings of each control method applied to the INSTAR system. Chapter 5 consists of the numerical

models for the M16 and its control designs. Chapter 6 presents the results of each control system derived in this study. Chapter 7 gives the conclusion of this study.

Chapter 2

Mathematical Model

This chapter discusses the actuator's design and how its constraints will be used in the development of the control design. It also includes the mathematical model which results from the system's equations of motion which are solved for using Newton's second law applied to the rotational inertias of the stock and barrel in the azimuth and elevation direction.

2.1 Actuator

INSTAR is a tactical rifle designed to address unwanted shooter-induced disturbances by decoupling their effects from the rifle's barrel via an active suspension system (Brei 2003). A free body diagram of the active suspension system including the mass of the rifle is shown in Figure 2.1 where W is the weight of the barrel. The active suspension system consists of restoring force F_s modeled as a spring of stiffness k_s , an actuator force F_a modeled as spring of stiffness k_a with an actuator displacement of x_a , sensors, and a power supply. Distances l_w , l_s , and l_a are the moment lengths of W , F_s , and F_a , respectively (Brei et. al 2003). These moment lengths are measured from the pivot point of the rifle located at the shooter's shoulder. These lengths will be used to derive the equations of motion for the rifle's dynamic model (Brei et. al 2003). Based on the feedback of the targeting error $\theta(t)$ from the sensors, a control system will calculate the desired x_a and F_a needed to cancel out the human disturbances that are imparted to the

rifle. The actuators are designed to cancel out jitter disturbances in a frequency range of 3Hz-5Hz.

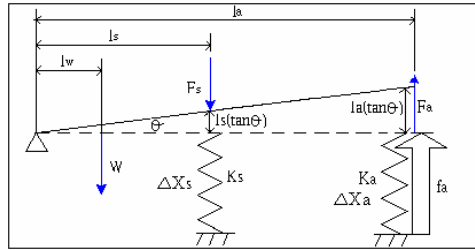


Figure 2.1: Free Body Diagram Including Shoulder and Arm Disturbance
(Brei et. al, 2003)

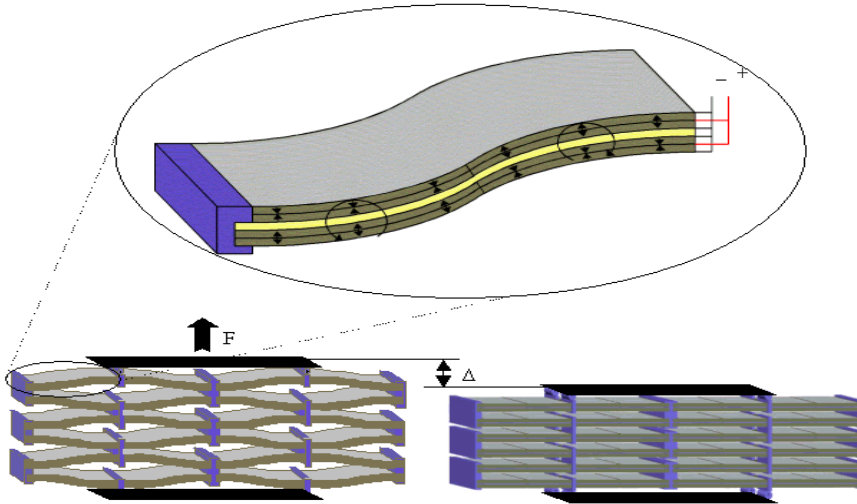


Figure 2.2: The Actuator's Piezoceramic Layers (Brei et. al, 2003)

The actuator itself is composed of multiple piezoceramic layers interconnected in series and/or parallel. A voltage applied to the array of layers produces a net push or pull

motion resulting in an applied force with a displacement Δ as labeled in Figure 2.2. The unique design of the actuator allows it to provide ample force and displacement and satisfy the size constraints of being able to fit into the stock of the rifle, while adding minimal amount of weight to the rifle (Brei et al, 2003)



Figure 2.3: Prototype Actuator for INSTAR (Brei et al, 2003)

The actuator moves the barrel in the elevation direction, producing a range of barrel angles θ . The actuator is designed to isolate a shooter induced disturbance from the gun barrel's point of aim for a stationary shooter with targeting error amplitude of 1.5 to 3 silhouettes at various ranges (Brei et. al 2003). If the shooter is located 400m from their designated target this equates to a targeting error θ , of 1.88mrad as shown in Figure 2.4.

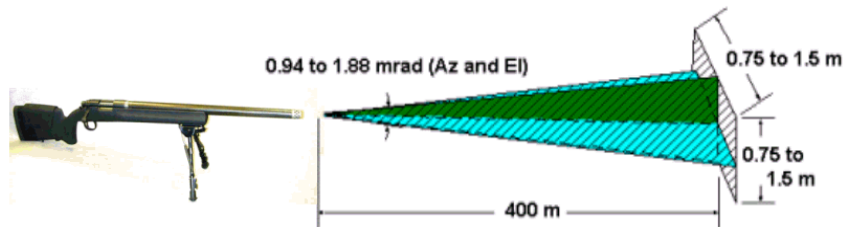


Figure 2.4: Allowable shooter targeting error range (Brei et. al, 2003)

Since the rifle is a portable system, the actuators are battery powered. The battery is a 9V DC source (Brei et. al, 2003) . Assuming the average on-time for the system to be 2 seconds, the actuator will be able to function for thousands of shots per fully charged battery.

Table 2.1 Actuator Specifications

Actuator Force(Max)	8N
Actuator Displacement (Max)	1.90mm
Power Supply	9V
Power Usage	2W
Weight	500g

2.2 Model Description

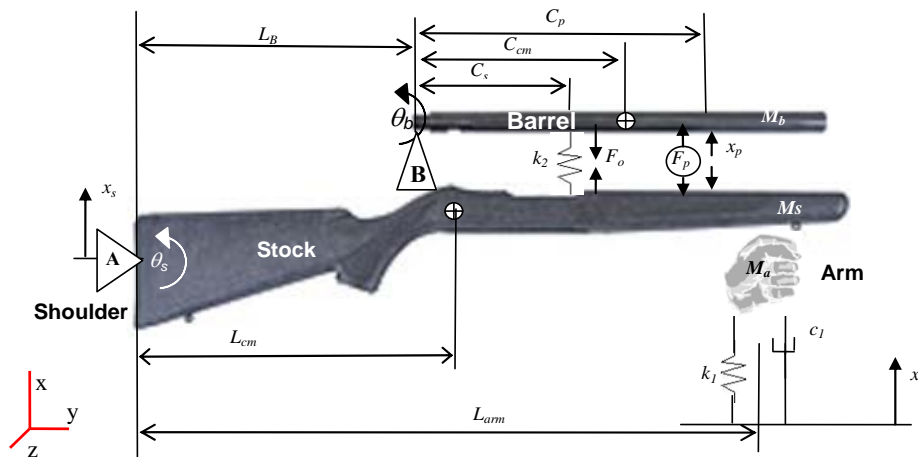


Figure 2.5: Generic Dynamic Model with Active Stabilization (Brei et. al, 2003)

Figure 2.5 is a generic analytical dynamic rifle model. It consists of the stock of the gun, the barrel of the gun, the active suspension stabilizing system, along with the human arm and shoulder disturbance.

The active suspension stabilizing system consists of the actuator which produces a force F_p at displacement x_p , and the preloaded restoring force F_o which is produced by spring constant k_2 which is located between the barrel and the stock of the weapon (Brei et. al, 2003). The active suspension stabilizing system serves to buffer out the jitter effects that result from human interaction with the weapon. The actuator moves the barrel of the rifle up and down independent of the stock while spring constant k_2 produces F_o to hold the barrel onto the actuator (Brei et. al, 2003).

The barrel and the stock are the two major components of a rifle. Their masses are so large that the masses of the other parts of the rifle are seen as negligible, therefore only the mass of the stock M_s and the mass of the barrel M_b are placed in the analytical dynamic model (Brei et. al, 2003). The stock of the rifle serves to facilitate easy steady holding and aiming of the rifle prior to and during firing of the rifle. The barrel of the rifle is a cylindrical metal tube through which the bullet travels before leaving the rifle.

The human disturbances are modeled at the two main points of human-rifle contact with respect to the x-y-z coordinate system shown in Figure 2.5. These points are where the shoulder and hand touch the rifle (Brei et. al 2003). The shoulder disturbance is modeled in Figure 2.5 with a pivot point of the rifle with an angle of θ_s , and a translation

in the positive direction due to shoulder disturbance is modeled as displacement x_s at the pivot point A (Brei et. al 2003). The arm disturbance is modeled as a mass-spring-damper system to account for the movements due to the musculature of the arm (Brei et. al 2003).

Figure 2.5 has two pivot points, θ_s , the angle of the stock and θ_b , the angle of the barrel. Both angles are measured relative to the horizontal, however θ_b is the angle of importance. The angle measured by θ_b corresponds to the targeting error of the rifle system (Brei et.al 2003). It is desired that θ_b be equal zero. The value of θ_b can be expressed in terms of θ_s and x_p as follows:

$$\theta_s = \theta_b - \frac{x_p}{C_p} \quad (2.1)$$

The equations of motion for the rifle were established by applying Newton's second law to the forces in the vertical direction in Figure 2.5. These equations of motion fully describe the motions of the rifle subject to base excitation inputs x_a , x_s and platform force input F_p (Brei, Luntz, Barnes, 2005).

$$\mathbf{M} \begin{bmatrix} \ddot{x}_p \\ \ddot{\theta}_b \end{bmatrix} + \mathbf{C} \begin{bmatrix} \dot{x}_p \\ \dot{\theta}_b \end{bmatrix} + \mathbf{K} \begin{bmatrix} x_p \\ \theta_b \end{bmatrix} = \mathbf{G}_s + \mathbf{G}_a + \mathbf{H}\mathbf{F}_p + \mathbf{D}\mathbf{F}_0 \quad (2.2)$$

where the mass matrix \mathbf{M} is

$$\mathbf{M} = \begin{bmatrix} \frac{-I_s + L_B^2 M_b}{C_p} & I_s + L_B M_b (L_B + C_{cm}) \\ \frac{-M_b C_{cm} L_B}{C_p} & I_{b,P} + M_b C_{cm} L_B \end{bmatrix}, \quad (2.3)$$

the damping matrix \mathbf{C} is

$$\mathbf{C} = \begin{bmatrix} \frac{-C_{arm} L_{arm}^2}{C_p} & C_{arm} L_{arm}^2 \\ 0 & 0 \end{bmatrix}, \quad (2.4)$$

the stiffness matrix \mathbf{K} is

$$\mathbf{K} = \begin{bmatrix} -\left(\frac{C_s^2 k_2 + k_1 L_{arm}^2}{C_p} \right) & k_1 L_{arm}^2 \\ \frac{k_2 C_s^2}{C_p} & 0 \end{bmatrix}, \quad (2.5)$$

the shoulder disturbance matrix \mathbf{G}_s is

$$\mathbf{G}_s = \begin{bmatrix} (-M_s L_{cm} M_b) \ddot{x}_s - L_{arm} C_{arm} \dot{x}_s - k_1 L_{arm} x_s \\ (-M_b C_{cm}) \ddot{x}_s \end{bmatrix}, \quad (2.6)$$

the arm disturbance matrix \mathbf{G}_a is

$$\mathbf{G}_a = \begin{bmatrix} L_{arm} C_{arm} \dot{x}_a + k_1 L_{arm} x_a \\ 0 \end{bmatrix}, \quad (2.7)$$

the moment matrix of the actuator is \mathbf{H}

$$\mathbf{H} = \begin{bmatrix} -C_p \\ C_p \end{bmatrix}, \quad (2.8)$$

and the matrix \mathbf{D} represents the moment arms for spring preload F_0

$$\mathbf{D} = \begin{bmatrix} C_s \\ -C_s \end{bmatrix} \quad (2.9)$$

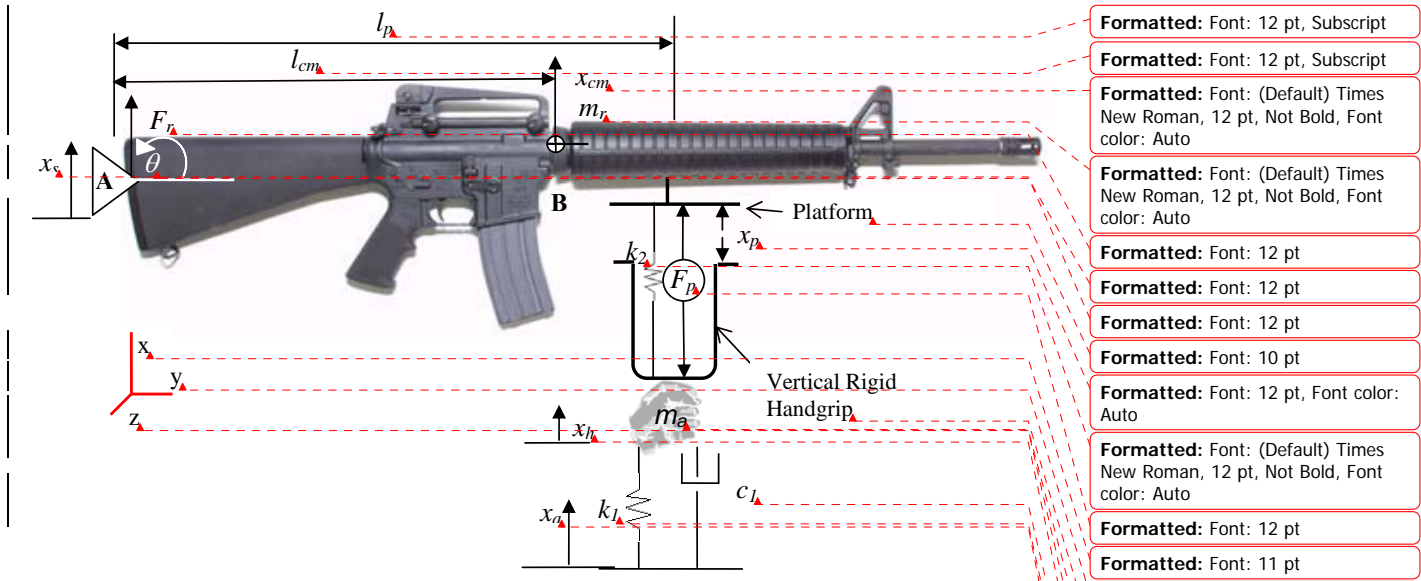


Figure 2.6: Dynamic M16 Combat Rifle Model with Active Stabilization (Brei et. al, 2005)

Figure 2.6 is the analytical dynamic model for the M16 Assault Rifle. Kinematically Figure 2.6 represents a different case from the generic model in Figure 2.5 in that its stock and barrel are rigidly attached, with the actuator held directly by the arm (Brei, et. al, 2005). Since the stock and barrel are rigidly attached their masses are summed together into M_b and the stock mass M_s is set to zero. Figure 2.6 only has one pivot point A so unlike Figure 2.5, the M16 has only one angle of rotation θ_b that is measured relative to the horizontal.

The equations of motion for the M16 are

- Formatted: Font: 12 pt, Subscript
- Formatted: Font: 12 pt, Subscript
- Formatted: Font: (Default) Times New Roman, 12 pt, Not Bold, Font color: Auto
- Formatted: Font: (Default) Times New Roman, 12 pt, Not Bold, Font color: Auto
- Formatted: Font: 12 pt
- Formatted: Font: 12 pt
- Formatted: Font: 12 pt
- Formatted: Font: 10 pt
- Formatted: Font: 12 pt, Font color: Auto
- Formatted: Font: (Default) Times New Roman, 12 pt, Not Bold, Font color: Auto
- Formatted: Font: 12 pt
- Formatted: Font: 11 pt
- Formatted: Font: 11 pt
- Formatted: Font: 10 pt
- Formatted: Font: 12 pt, Not Bold
- Formatted: Font: 11 pt
- Formatted: Font: 12 pt

$$\mathbf{M} \begin{bmatrix} \ddot{x}_p \\ \ddot{\theta}_b \end{bmatrix} + \mathbf{C} \begin{bmatrix} \dot{x}_p \\ \dot{\theta}_b \end{bmatrix} + \mathbf{K} \begin{bmatrix} x_p \\ \theta_b \end{bmatrix} = \mathbf{G}_s + \mathbf{G}_a + \mathbf{H}\mathbf{F}_p, \quad (2.10)$$

where the mass matrix \mathbf{M} is

$$\mathbf{M} = \begin{bmatrix} -m_a & m_a l_p \\ 0 & I_A \end{bmatrix}, \quad (2.11)$$

the damping matrix \mathbf{C} is

$$\mathbf{C} = \begin{bmatrix} -c_1 & c_1 l_p \\ 0 & 0 \end{bmatrix}, \quad (2.12)$$

the stiffness matrix \mathbf{K} is

$$\mathbf{K} = \begin{bmatrix} -(k_1 + k_2) & k_1 l_p \\ k_2 l_p & 0 \end{bmatrix}, \quad (2.13)$$

the shoulder disturbance matrix \mathbf{G}_s is

$$\mathbf{G}_s = \begin{bmatrix} -m_a \ddot{x}_s - c_1 \dot{x}_s - k_1 x_s \\ -m_r l_{cm} \ddot{x}_s \end{bmatrix}, \quad (2.14)$$

the arm disturbance matrix \mathbf{G}_a is

$$\mathbf{G}_a = \begin{bmatrix} -c_1\dot{x}_a - k_1x_a \\ 0 \end{bmatrix}, \quad (2.15)$$

and the moment matrix of the actuator is \mathbf{H}

$$\mathbf{H} = \begin{bmatrix} -1 \\ l_p \end{bmatrix}, \quad (2.16)$$

2.3 M16 State Space

A plant design of the M16's dynamics must be developed before control theory may be applied to the system. The plant is a mathematical model that fully captures the dynamics of the M16 rifle while taking into consideration the rifle's response to human interaction. Equations (2.10-2.16) will be used to develop the plant model since these equations fully describe the motions of the rifle being shot by a human in a stationary position (Brei et. al, 2005).

The desired form of the system is

$$\begin{aligned} \mathbf{x}(t) &= \mathbf{A}\mathbf{x}(t) + \mathbf{B}\mathbf{u}(t) + \mathbf{d}(t), & \mathbf{x}(t) \in R^n, & \mathbf{u}(t) \in R^m \\ \mathbf{y}(t) &= \mathbf{C}\mathbf{x}(t) \end{aligned} \quad (2.17)$$

Where n represents the number of states and m represents the number of system inputs, $\mathbf{A} \in R^{n \times n}$ is the state (plant) matrix, $\mathbf{x}(t)$ is the state vector, $\mathbf{B} \in R^{n \times m}$ is the input matrix, $\mathbf{u}(t)$ is the input vector, $\mathbf{d}(t)$ is the disturbance vector, and \mathbf{C} is the output matrix.

The dynamic equations for the M16 mass-damper-spring system are given by

$$\begin{bmatrix} -m_a & m_a l_p \\ 0 & I_A \end{bmatrix} \begin{bmatrix} \ddot{x}_p \\ \ddot{\theta} \end{bmatrix} + \begin{bmatrix} -c_l & c_l l_p \\ 0 & 0 \end{bmatrix} \begin{bmatrix} \dot{x}_p \\ \dot{\theta} \end{bmatrix} + \begin{bmatrix} -(k_1 + k_2) & k_1 l_p \\ k_2 l_p & 0 \end{bmatrix} \begin{bmatrix} x_p \\ \theta \end{bmatrix} =$$

(2.18)

$$\begin{bmatrix} -1 \\ l_p \end{bmatrix} F_p(t) + \begin{bmatrix} -k_1 x_a - c_l \dot{x}_a \\ 0 \end{bmatrix} + \begin{bmatrix} -m_a \ddot{x}_s - c_1 \dot{x}_s - k_1 x_s \\ -m_r l_{cm} \ddot{x}_s \end{bmatrix}$$

The last two terms in Equation (2.18) are essentially disturbances imparted by the shooter to the gun. They are modeled as disturbance signals

$$d_1(t) = -k_1 x_a - c_l \dot{x}_a - m_a \ddot{x}_s - c_1 \dot{x}_s - k_1 x_s \quad (2.19)$$

$$d_2(t) = -m_r l_{cm} \ddot{x}_s \quad (2.20)$$

In Equation (2.19), $d_1(t)$ is a combination of arm disturbance x_a and shoulder disturbance x_s . Equation (2.20) is only composed of shoulder disturbance x_s . When the shooter holds the gun, ergonomic disturbances cause the gun barrel to oscillate. Disturbances $d_1(t)$ and $d_2(t)$ are assumed to be sinusoidal of the form

$$d_1(t) = A_1 \sin(\omega_1 t) \quad (2.21)$$

$$d_2(t) = A_2 \sin(\omega_1 t) \quad (2.22)$$

Equation (2.18) can now be written as

$$\begin{aligned} & \begin{bmatrix} -m_a & m_a l_p \\ 0 & I_A \end{bmatrix} \begin{bmatrix} \ddot{x}_p \\ \ddot{\theta} \end{bmatrix} + \begin{bmatrix} -c_l & c_l l_p \\ 0 & 0 \end{bmatrix} \begin{bmatrix} \dot{x}_p \\ \dot{\theta} \end{bmatrix} + \begin{bmatrix} -(k_1 + k_2) & k_1 l_p \\ k_2 l_p & 0 \end{bmatrix} \begin{bmatrix} x_p \\ \theta \end{bmatrix} \\ & = \begin{bmatrix} -1 \\ l_p \end{bmatrix} F_p(t) + \begin{bmatrix} A_1 \sin(\omega_1 t) \\ A_2 \sin(\omega_1 t) \end{bmatrix} \end{aligned} \quad (2.23)$$

Equation (2.23) can be put into state space form so that control theory may be applied to enhance the performance of the system. Equation (2.26) is multiplied by

$$\begin{bmatrix} -m_a & m_a l_p \\ 0 & I_A \end{bmatrix}^{-1} \text{ so that } \begin{bmatrix} \ddot{x}_p \\ \ddot{\theta} \end{bmatrix}^T \text{ is the lone term on the left side of the equation.}$$

The resulting equation is

$$\begin{aligned} & \begin{bmatrix} \ddot{x}_p \\ \ddot{\theta} \end{bmatrix} + \begin{bmatrix} -m_a & m_a l_p \\ 0 & I_A \end{bmatrix}^{-1} \begin{bmatrix} -c_l & c_l l_p \\ 0 & 0 \end{bmatrix} \begin{bmatrix} \dot{x}_p \\ \dot{\theta} \end{bmatrix} + \begin{bmatrix} -m_a & m_a l_p \\ 0 & I_A \end{bmatrix}^{-1} \begin{bmatrix} -(k_1 + k_2) & k_1 l_p \\ k_2 l_p & 0 \end{bmatrix} \begin{bmatrix} x_p \\ \theta \end{bmatrix} \\ & = \begin{bmatrix} -m_a & m_a l_p \\ 0 & I_A \end{bmatrix}^{-1} \begin{bmatrix} -1 \\ l_p \end{bmatrix} F_p(t) + \begin{bmatrix} -m_a & m_a l_p \\ 0 & I_A \end{bmatrix}^{-1} \begin{bmatrix} A_1 \sin(\omega_1 t) \\ A_2 \sin(\omega_1 t) \end{bmatrix} \end{aligned} \quad (2.24)$$

The matrix $\begin{bmatrix} -m_a & m_a l_p \\ 0 & I_A \end{bmatrix}^{-1}$ is a diagonal matrix, therefore its inverse does exist.

After multiplying out the matrices, equation (2.24) becomes

$$\begin{aligned}
\begin{bmatrix} \ddot{x}_p \\ \ddot{\theta} \end{bmatrix} &= (-1) \begin{bmatrix} \frac{c_1}{m_a} & \frac{-c_1 l_p}{m_a} \\ 0 & 0 \end{bmatrix} \begin{bmatrix} \dot{x}_p \\ \dot{\theta} \end{bmatrix} + (-1) \begin{bmatrix} \frac{I_A(k_1 + k_2) + m_a l_p^2 k_2}{I_A m_a} & \frac{-k_1 l_p}{m_a} \\ \frac{k_2 l_p}{I_A} & 0 \end{bmatrix} \begin{bmatrix} x_p \\ \theta \end{bmatrix} \\
&= \begin{bmatrix} \frac{I_A + m_a l_p^2}{I_A m_a} \\ \frac{l_p}{I_A} \end{bmatrix} F_p(t) + \begin{bmatrix} -1 & \frac{l_p}{I_A} \\ \frac{1}{m_a} & 0 \end{bmatrix} \begin{bmatrix} A_1 \sin(\omega_1 t) \\ A_2 \sin(\omega_1 t) \end{bmatrix}
\end{aligned} \tag{2.25}$$

$$\begin{bmatrix} \ddot{x}_p \\ \ddot{\theta} \end{bmatrix} = (-1) \begin{bmatrix} a & b \\ 0 & 0 \end{bmatrix} \begin{bmatrix} \dot{x}_p \\ \dot{\theta} \end{bmatrix} + (-1) \begin{bmatrix} e & f \\ g & 0 \end{bmatrix} \begin{bmatrix} x_p \\ \theta \end{bmatrix} + \begin{bmatrix} h \\ i \end{bmatrix} F_p(t) + \begin{bmatrix} j & k \\ 0 & l \end{bmatrix} \begin{bmatrix} d_1(t) \\ d_2(t) \end{bmatrix} \tag{2.26}$$

where

$$\begin{aligned}
a &= \frac{c_1}{m_a}, b = \frac{-c_1 l_p}{m_a}, e = \frac{I_A(k_1 + k_2) + m_a l_p^2 k_2}{I_A m_a}, f = \frac{-k_1 l_p}{m_a}, g = \frac{k_2 l_p}{I_A} \\
h &= \frac{I_A + m_a l_p^2}{I_A m_a}, i = \frac{l_p}{I_A}, j = \frac{-1}{m_a}, k = \frac{l_p}{I_A}, l = \frac{1}{I_A}
\end{aligned} \tag{2.27}$$

To model equation (2.26) into a state space model the state variables are defined

as

$$\begin{aligned}
x_1 &= x_p, \quad x_2 = \dot{x}_p, \quad y_1 = \theta, \quad y_2 = \dot{\theta} \\
\dot{x}_1 &= x_2 \\
\dot{x}_2 &= -a(x_2) - b(y_2) - e(x_1) - f(y_1) + h(F_p(t)) + j(d_1(t)) + k(d_2(t)) \\
\dot{y}_1 &= y_2 \\
\dot{y}_2 &= -g(x_1) + i(F_p(t)) + l(d_2(t))
\end{aligned} \tag{2.28}$$

With these state variables the second order dynamic equations in equation (2.28) can be formed into the desired form of a state space model

$$\begin{bmatrix} \dot{x}_1(t) \\ \dot{x}_2(t) \\ \dot{y}_1(t) \\ \dot{y}_2(t) \end{bmatrix} = \underbrace{\begin{bmatrix} 0 & 1 & 0 & 0 \\ -e & -a & -f & -b \\ 0 & 0 & 0 & 1 \\ -g & 0 & 0 & 0 \end{bmatrix}}_{\mathbf{A}} \begin{bmatrix} x_1(t) \\ x_2(t) \\ y_1(t) \\ y_2(t) \end{bmatrix} + \underbrace{\begin{bmatrix} 0 \\ h \\ 0 \\ i \end{bmatrix}}_{\mathbf{B}} [F_p(t)] + \begin{bmatrix} 0 & 0 \\ j & k \\ 0 & 0 \\ 0 & l \end{bmatrix} \begin{bmatrix} d_1(t) \\ d_2(t) \end{bmatrix} \tag{2.29}$$

$$[\theta(t)] = \underbrace{\begin{bmatrix} 0 & 0 & 1 & 0 \end{bmatrix}}_{\mathbf{C}} \begin{bmatrix} x_1(t) \\ x_2(t) \\ y_1(t) \\ y_2(t) \end{bmatrix}$$

The system represented by equation (2.29) outputs the barrel angle $\theta(t)$. Equation (2.29) is a fourth order state space dynamic model of an M16, where the motion is introduced by a shooter's arm and shoulder disturbance, and the actuator force that is required to reduce the amplitude of movement of the M16's barrel.

In equation (2.29) the state space representation of the M16's dynamic model, matrix A represents the plant matrix of the M16 which represents the behavior of the states of the system. The state's behavior that will be closely monitored is $x_1(t)$ which is equal to $x_p(t)$, the measurable value of the actuator's displacement. Matrix B in equation (2.29) represents the behavior of the system's input $F_p(t)$. Matrix C in equation (2.29) is the output matrix of system. It outputs the rifle's barrel angle $\theta(t)$ which is also referred to as the targeting error.

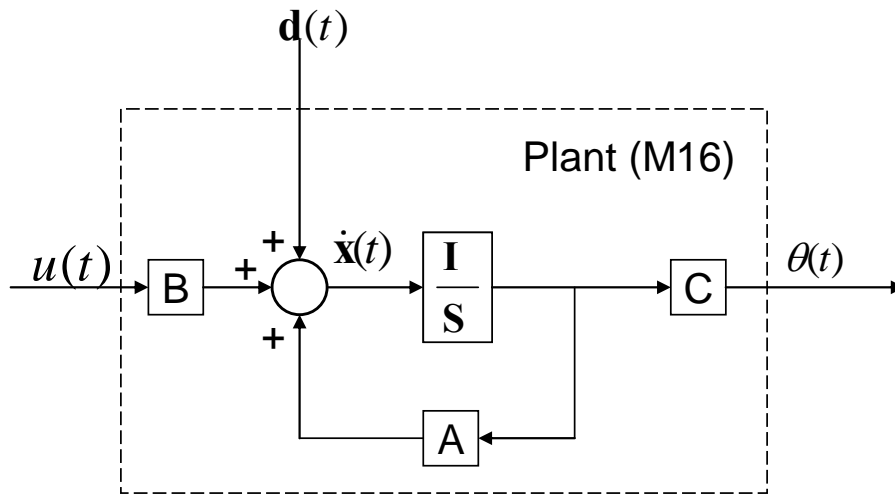


Figure 2.7: Block diagram of equation 2.29

Figure 2.7 is a block diagram of the M16's dynamic model without a controller applied to the system. In Figure 2.7 $u(t)$ is the control input which corresponds to the barrel stabilizing actuator force $F_p(t)$. For all systems in this paper with or without a controller, $u(t)$ represents the stabilizing actuator input $F_p(t)$. Since equation (2.29)

represents a linear time invariant system, the laplace transform may be used to calculate the system's transfer function, in the frequency domain. The transfer function of the system is based on the relationship between input $F_p(t)$, with respect to the system output $\theta(t)$.

$$\frac{Y(s)}{U(s)} = C(sI - A)^{-1}B + D \quad (2.30)$$

Equation (2.30) is the transfer function of the system. The transfer function of the system describes many characteristics of the system. Characteristics including the order of the system, the stability of the system, the transient response of the system, and the steady state response of the system. These tools will be used to evaluate and compare the performance of the system with and without control compensation.

Chapter 3

Design Criteria

This chapter is a collection of the specifications and criteria that must be met by all control systems that are designed in this paper. It discusses how the specifications of the actuator in Chapter 2 are converted to constraints that the designed control systems must meet. Meeting criteria ensures that the control systems designed are practical and that they are able to function properly with all components of the active stabilization system.

3.1 Constraints and Specifications

The value of $x_p(t)$ limits the targeting error allowed by the shooter. The maximum displacement value of the actuator is $x_p(t) = 1.90 \text{ mm}$ (Brei et. al, 2003). In order for the actuator to properly cancel out the aiming errors of the shooter, the shooter must be able to come within 3 silhouettes of the target at a maximum range of 250m. This is equal to a target error distribution of (Brei et. al, 2003). In Figure 3.1, the allowable target error distribution by the shooter is represented by the shaded region.

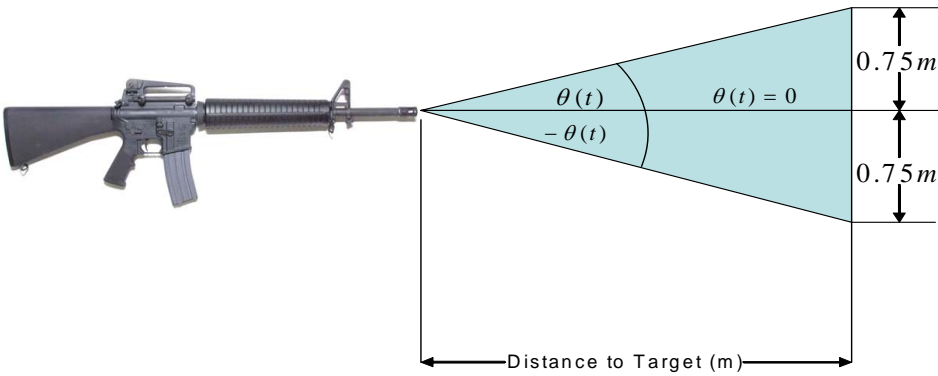


Figure 3.1: Targeting Error Distribution

Upon getting into position and acquiring the target, the shooter activates the control system. Within a short amount of time the control system acts to cancel out the jitters imparted on the rifle barrel by the shooter. This action dramatically increases the accuracy of the shooter. The time from which the shooter activates the control system to when the shooter actually pulls the trigger has to be done in 1s (Brei et. al, 2003). This is called Time To Trigger Pull (T^3P). Maintaining a T^3P of 1s or less preserves the battery life of the active stabilization system, enabling the system to operate for thousands of shots.

The maximum magnitude of actuator force is 8N (Brei et. al, 2003). This corresponds to a control input range of $u(t) \leq 8N$. All control designs for the M16 rifle must meet this constraint to prevent saturation of the actuator.

The frequency of observation for the shooter induced disturbances is 3Hz (Brei et. al 2003). It is at this frequency that the control system must be able to decrease the targeting error of the shooter.

Table 3.1 Maximum values of control constraints and specifications

Disturbances	3Hz
Targeting Error	0.75m
$u(t)$	8N
$x_p(t)$	1.9mm
T ³ P	1s

Chapter 4

Control Techniques

Through analysis of the nominal plant's root locus and transfer function, various control techniques are suggested to properly reduce the jitter effects upon the rifle due to human interaction with the weapon. This chapter consists of the motivation behind each controller design.

4.1 Unity Feedback Gain

Applying unity feedback gain to the plant is the initial control technique used to reduce human induced targeting error. Since the output of the plant was sinusoidal it was decided to feed the output back into the system. Multiplying the feedback by a negative unity gain, produces an error signal that is fed back into the system, in hopes that the system will subtract this error signal from the output to produce better results as time passes. Simplicity is the main contributor behind the motivation of using a unity feedback loop. The unity feedback controller applied to the M16 plant is shown in Figure 4.1. The hardware design of a feedback gain control system can be accomplished by connecting a wire from the system output to the system input.

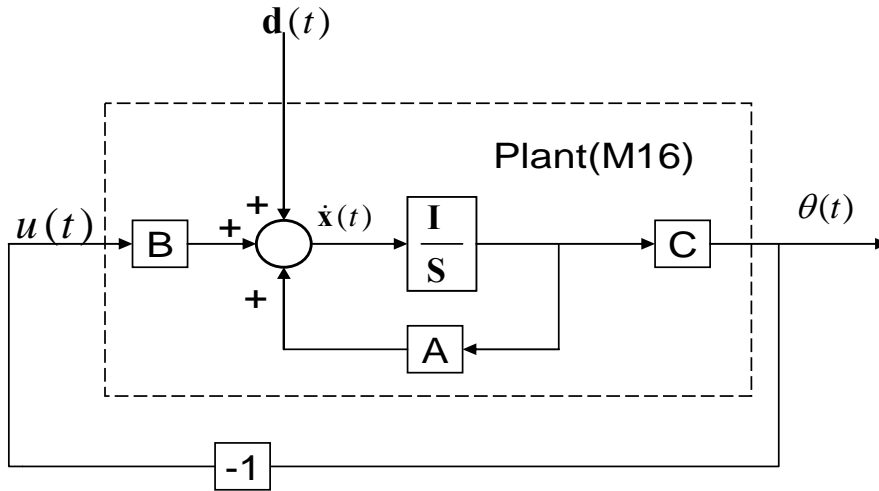


Figure 4.1: Negative Unity Feedback Control System

The open loop state space equation for Figure 4.1 is

$$\begin{aligned}\dot{\mathbf{x}}(t) &= \mathbf{A}\mathbf{x}(t) + \mathbf{B}u(t) + \mathbf{d}(t) \\ y(t) &= \mathbf{C}\mathbf{x}(t)\end{aligned}\quad (4.1)$$

and the control law for Figure 4.1 is

$$u(t) = -\mathbf{C}\mathbf{x}(t)\quad (4.2)$$

After substituting equation (4.2) into (4.1) the closed loop equation becomes

$$\begin{aligned}\dot{\mathbf{x}}(t) &= (\mathbf{A} - \mathbf{B}\mathbf{C})\mathbf{x}(t) + \mathbf{d}(t) \\ y(t) &= \mathbf{C}\mathbf{x}(t)\end{aligned}\quad (4.3)$$

The state matrix of equation (4.3) is

$$\mathbf{A} - \mathbf{B}\mathbf{C}\quad (4.4)$$

The eigenvalues of equation (4.4) describe the stability of the unity feedback system in Figure 4.1.

4.2 Compensator

Assuming that the transfer function of the M16 system

$$H(s) = \frac{Y(s)}{U(s)} \quad (4.5)$$

has complex poles of the form $p_i = \alpha_i + \omega_i j$ $i = \{1, 2, \dots, n\}$, with small damping. These open loop complex poles p_i are to the left of and close to the $j\omega$ -axis. A system that has complex poles close to the $j\omega$ axis has an unfavorable characteristic of being marginally stable. In addition to this, complex poles with small damping produce large unwanted resonated oscillations in the system's frequency response at their corresponding frequencies ω_i . The undesirable performance characteristics of a system being marginally stable and having small damping can be reduced through phase compensation by a compensator. The phase compensation control system will consist of the transfer function $H(s)$ cascaded with a scalar gain K and a dynamic compensator $C(s)$ as shown in Figure 4.2.

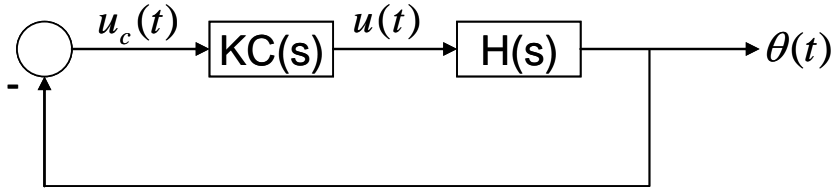


Figure 4.2: Control system w/negative unity feedback

Let ϕ_i be the departure angle of p_i and ϕ_{di} be the desired departure angle of p_i .

The desired departure angle of p_i can be written as

$$\phi_{di} = \phi_i + \arg(C(p_i)) \quad (4.6)$$

Using standard complex function theory

$$\arg(C(j\omega_i)) \approx \arg(C(p_i)) \quad (4.7)$$

when α_i is small. Equation (4.6) shows the relationship between the phase of the compensator $C(j\omega_i)$ at the resonant frequency ω_i of complex pole p_i , the initial departure angle of p_i , and the desired departure angle of p_i (Lindner, Celano, Ide, 1991). After the compensator is designed, a Bode plot is used to analyze the

compensator's phase $\arg(C(j\omega_i))$ at the complex pole's resonant frequency ω_i of concern (Lindner et. al, 1991).

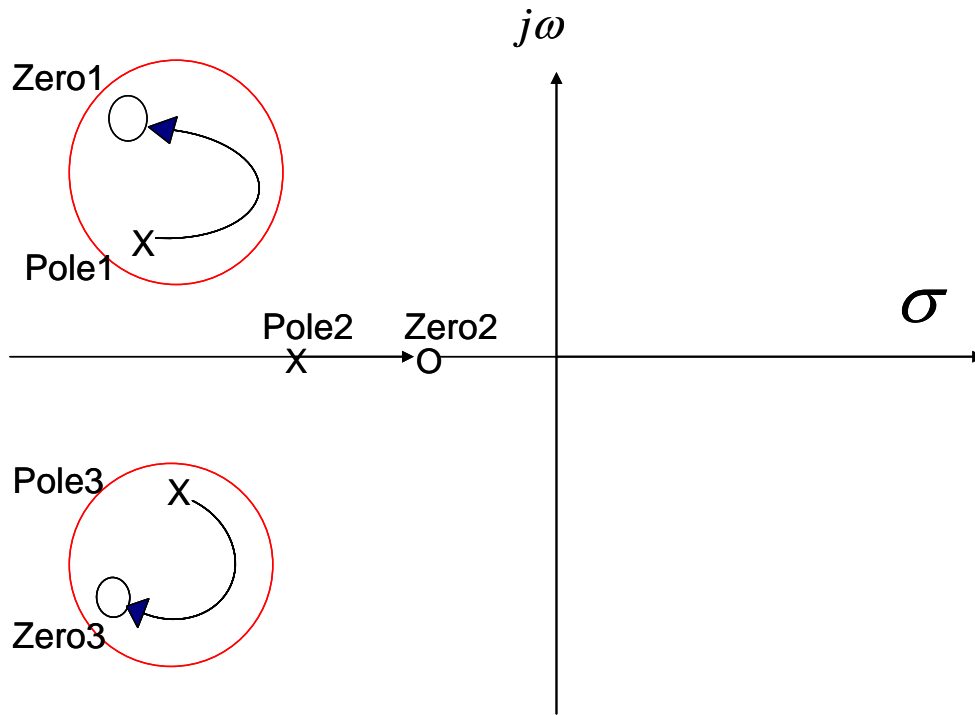


Figure 4.3: Generic Root Locus with two Complex Poles

The desired departure angle of the two complex poles is 180° . The compensator will be designed to change the departure angle of the complex poles. A departure angle of 180° will ensure that the system's open loop poles as well as the closed loop poles remain to the left of the $j\omega$ -axis thus ensuring that the system remains stable, and preventing the system's frequency response from resonating at the frequencies of the

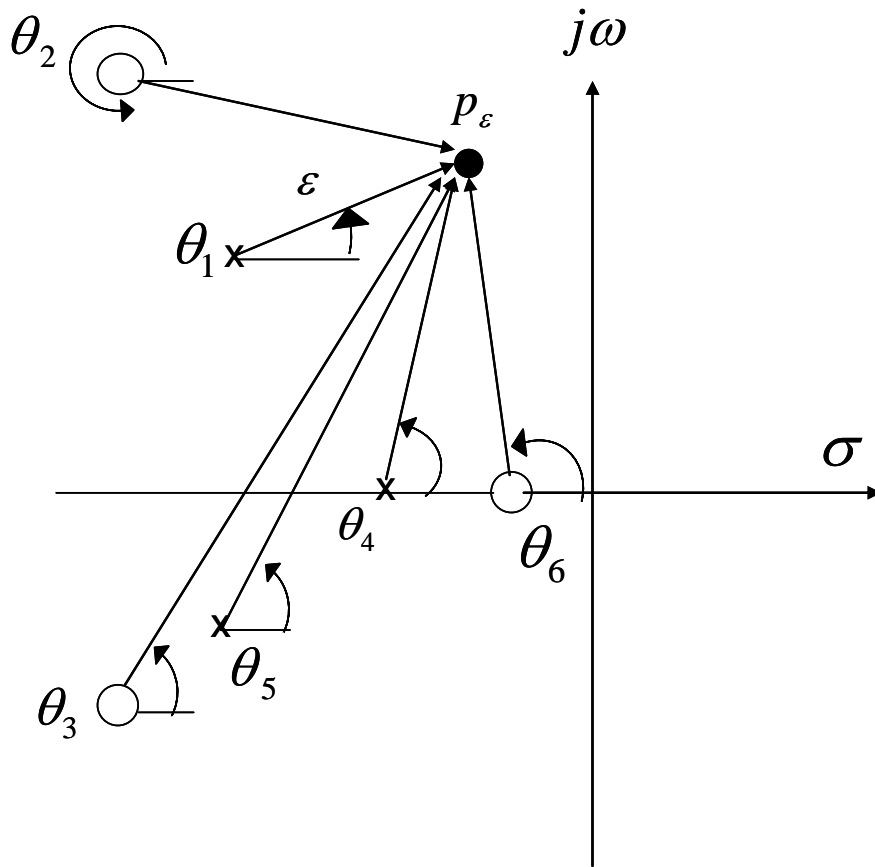
complex poles close to the $j\omega$ -axis. A departure angle of 180° will produce a stable system with a much lesser response time, while reducing the jitter in the system's transient response.

The departure angle of the root locus from the open loop pole, is measured relative to the real axis σ from the right. A departure angle of 90° is straight up vertical line, where as, a departure angle of 180° is a straight horizontal line directed towards the left. If a point is on the root locus, then the sum of all angles drawn from all finite poles and zeros to this point is an odd multiple of 180° . This property of the root locus is used to calculate the departure angle of the system's complex poles.

The total angle contribution of all finite zeros and poles towards a point located on the root locus equals $(2k + 1)180^\circ$ (where k is an integer). This is computed using equation (4.8).

$$\sum \angle_{zeros} - \sum \angle_{poles} = (2k + 1)180^\circ \quad (4.8)$$

The first step in calculating the departure angle from a pole on the root locus, is to place a point that is a extremely short ε distance away. This point is labeled as p_ε as shown in Figure 4.4. The departure angle, θ_1 of the root locus line is drawn from the open loop pole (Pole 1), to p_ε . The assumption that p_ε is located on the root locus, means that all lines drawn from the finite poles and zeros to p_ε have an angle sum of $(2k + 1)180^\circ$.

Figure 4.4: Generic Root Locus w/point p_ϵ

From equation (4.8) the summation of angles for a point on the root locus in Figure 4.4 is

$$-\theta_1 + \theta_2 + \theta_3 - \theta_4 - \theta_5 + \theta_6 = (2k + 1)180^\circ \quad (4.9)$$

The departure angle θ_1 can be solved for from equation (4.9).

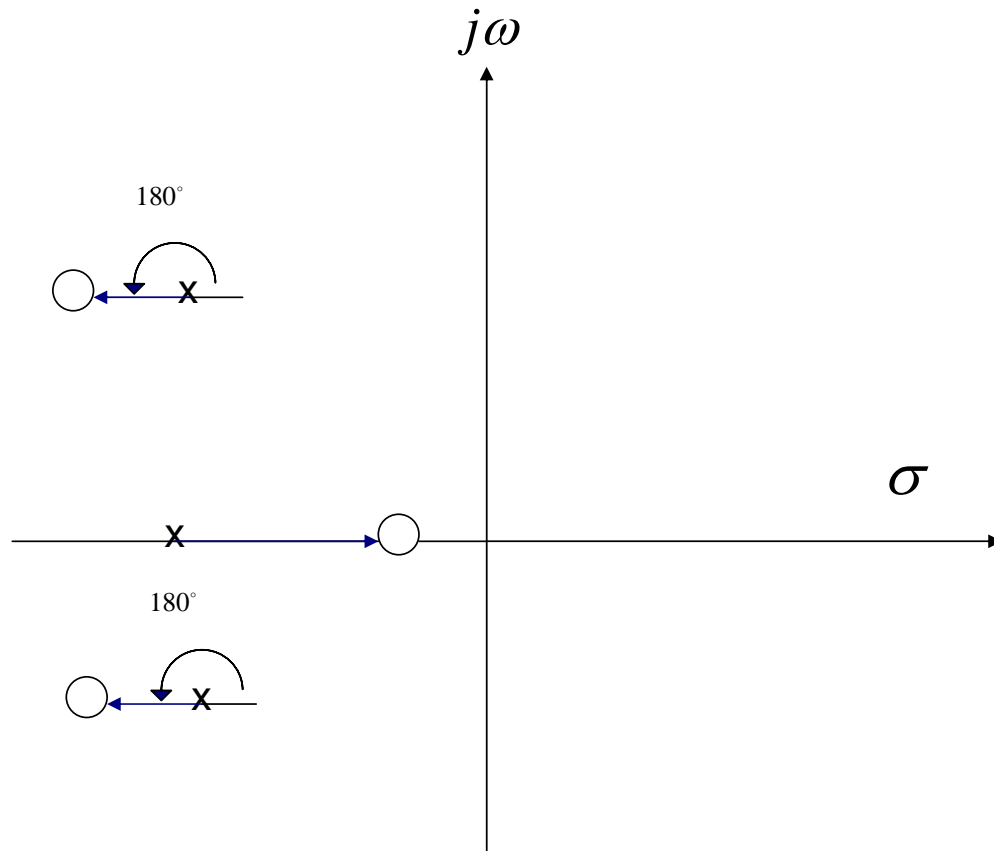


Figure 4.5: Generic Root Locus w/180 degree departure angle

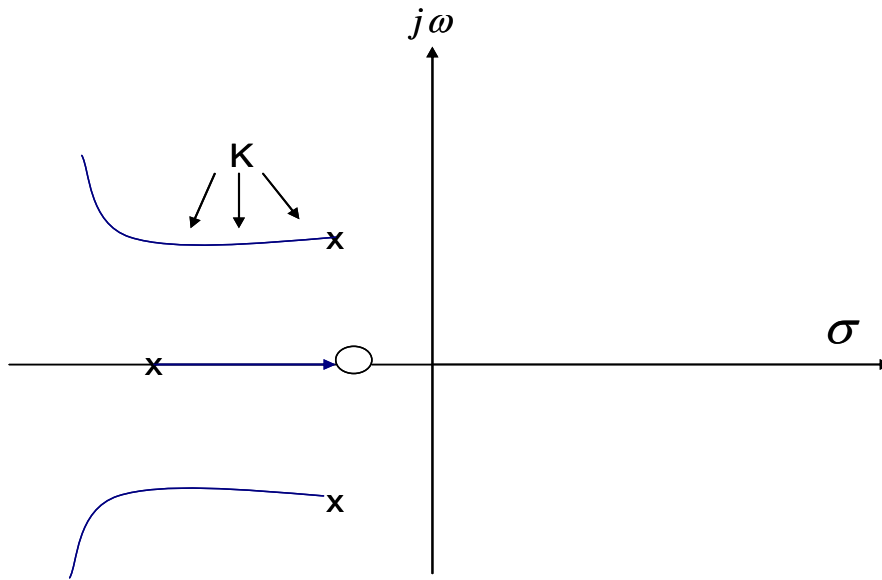


Figure 4.6: Possible K Values

After phase modification of complex poles via compensator design the scalar gain K of Figure 4.6 is selected by looking at the lines of the root locus of the system and choosing a point on the root locus. The suitable scalar gain K is chosen at the designer's discretion to produce the desired performance of the system. Figure 4.6 shows possible desirable K values that a designer may choose to incorporate into the control system. It is suggested that the designer choose K values where the departure angle of the root locus is 180° . The scalar K , in conjunction with compensator $C(s)$, helps to ensure a desired departure angle from the system's complex poles. Various gains K , may be chosen and simulated before satisfactory results are produced.

In Figure 4.2 the equation for the plant with transfer function $H(s)$ is

$$\begin{aligned}\dot{\mathbf{x}}_p(t) &= \mathbf{A}_p \mathbf{x}_p(t) + \mathbf{B}_p \mathbf{u}(t) + \mathbf{d}(t) \\ \mathbf{y}_p(t) &= \mathbf{C}_p \mathbf{x}_p(t)\end{aligned}\quad (4.10)$$

and the equation for the model of the compensator is

$$\begin{aligned}\dot{\mathbf{x}}_c(t) &= \mathbf{A}_c \mathbf{x}_c(t) + \mathbf{B}_c \mathbf{u}_c(t) \\ \mathbf{y}_c(t) &= \mathbf{C}_c \mathbf{x}_c(t) + \mathbf{D}_c \mathbf{u}_c(t)\end{aligned}\quad (4.11)$$

The control law for the plant is

$$u(t) = y_c(t)\quad (4.12)$$

and the control law for the compensator is

$$u_c(t) = -Ky_p(t)\quad (4.13)$$

After substituting equations (4.12) and (4.13) into equations (4.10) and (4.11), the closed loop state equation for the compensated system is

$$\begin{bmatrix} \dot{\mathbf{x}}_p(t) \\ \dot{\mathbf{x}}_c(t) \end{bmatrix} = \begin{bmatrix} \mathbf{A}_p - \mathbf{B}_p \mathbf{D}_c \mathbf{K} \mathbf{C}_p & \mathbf{B}_p \mathbf{C}_c \\ -\mathbf{B}_c \mathbf{K} \mathbf{C}_p & \mathbf{A}_c \end{bmatrix} \begin{bmatrix} \mathbf{x}_p(t) \\ \mathbf{x}_c(t) \end{bmatrix} + \begin{bmatrix} \mathbf{I} \\ \mathbf{0} \end{bmatrix} \mathbf{d}(t) \quad (4.14)$$

$$\mathbf{y}(t) = \begin{bmatrix} \mathbf{y}_p(t) \\ \mathbf{y}_c(t) \end{bmatrix} = \begin{bmatrix} \mathbf{C}_p & \mathbf{0} \\ -\mathbf{D}_c \mathbf{K} \mathbf{C}_p & \mathbf{C}_c \end{bmatrix} \begin{bmatrix} \mathbf{x}_p(t) \\ \mathbf{x}_c(t) \end{bmatrix}$$

The steps to the Compensator design for a system represented by Figure 4.2 are as follows (Lindner et. al 1991):

- (1) Determine the departure angles ϕ_i
- (2) Determine the desired compensator angles ϕ_{di} , usually 180°
- (3) Determine the desired compensator phase $C(j\omega_i)$ from equation (4.6) to achieve ϕ_{di} for $i=\{1,..m\}$ m = the number of complex poles
- (4) Synthesize an appropriate compensator, $C(j\omega_i)$ to satisfy step (3)
- (5) Using the root locus, determine a suitable gain K for the compensator

After following the steps the designed compensator should have a desirable affect on the departure angle from the poles. The closed loop complex poles will move away from the $j\omega$ axis, dampening their vibrations in the system's frequency response. The compensator moves these complex closed loop poles without significantly moving the other poles of the system. The compensator's magnitude is a key element to this behavior. It must be chosen so that the designer may move the desired poles without affecting the other poles of the system. This is important for the stability and performance of the compensated system.

4.3 State Feedback Matrix Gain

After analysis of a system's root locus and the system's time response, it may be decided by the designer that the system needs to converge to a smaller acceptable targeting error $\theta(t)$, in a shorter amount of time. Moving the open loop poles of the system further to the left of the $j\omega$ -axis will shorten the transient response of the system. In addition to being moved further to the left of the $j\omega$ -axis, complex poles must also be moved closer to the real axis thereby shortening the system's transient response and lowering the amplitude of the system's frequency response, thus producing a steady state error that meets specification. A state feedback matrix can be designed to place the system's poles in the new desired pole locations.

$$p_{i_d} \quad i = 1, \dots, n \quad (4.15)$$

Where n represents the number of open loop poles. This feedback matrix may be placed in a negative feedback loop. Adding a state feedback matrix controller to the system will hopefully improve how well the system's performance measures up to the established criteria. In some cases a feedback loop may cause the system to become unstable. A state feedback matrix may even allow the system to perform in a consistent and desired manner despite unaccounted for dynamic external affects that the system may experience in real world applications.

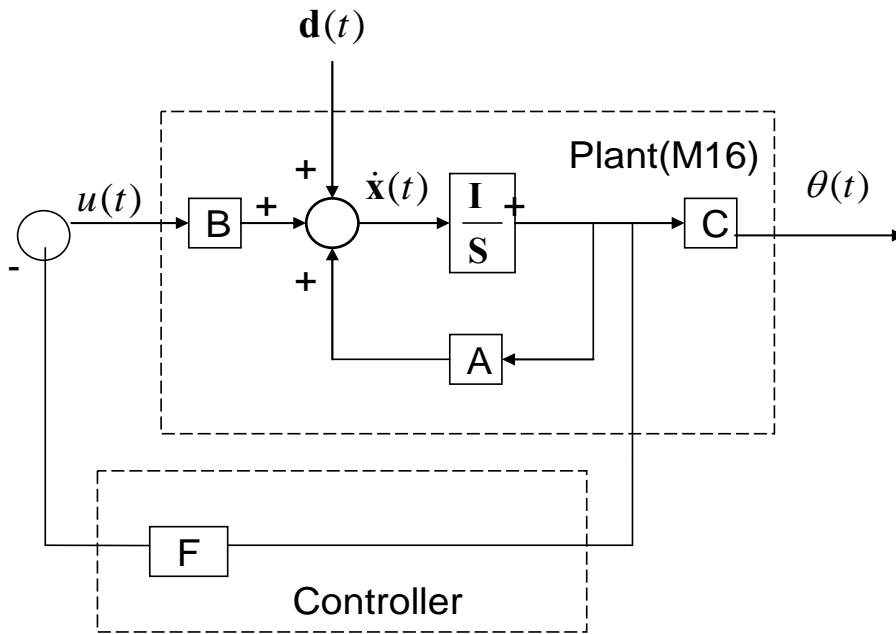


Figure 4.7: Plant with state feedback matrix

Consider the system

$$\begin{aligned}\dot{\mathbf{x}}(t) &= \mathbf{A}\mathbf{x}(t) + \mathbf{B}u(t) + \mathbf{d}(t) \\ \mathbf{y}(t) &= \mathbf{C}\mathbf{x}(t)\end{aligned}\quad (4.16)$$

In reference to equation (4.16) and Figure 4.7, the control law for this particular system is

$$u(t) = -\mathbf{F}\mathbf{x}(t)\quad (4.17)$$

After substituting equation (4.17) into equation (4.16), the closed loop system becomes

$$\begin{aligned}\dot{\mathbf{x}}(t) &= (\mathbf{A} - \mathbf{BF})\mathbf{x}(t) + \mathbf{d}(t) \\ \mathbf{y}(t) &= \mathbf{C}\mathbf{x}(t)\end{aligned}\quad (4.18)$$

The eigenvalues $\lambda(\mathbf{A} - \mathbf{BF})$ of the state matrix represent the pole locations of the closed loop system. In order to place the system's closed loop poles in desired locations, the eigenvalues of the closed loop system must be studied. The characteristic polynomial $p_d(s)$, of the desired close loop pole locations is

$$p_d(s) = (s - \lambda_{d1})(s - \lambda_{d2})\dots(s - \lambda_{dn}) = s^n + a_{d,n-1}s^{n-1} + a_{d,n-2}s^{n-2} + \dots + a_{d0} \quad (4.19)$$

where $\lambda_{d1}, \lambda_{d2}, \dots, \lambda_{dn} \in \Lambda_d$ are the eigenvalues of the desired system.

Theorem 4.1 *Upon proof that equation (4.16) is controllable, there exists a feedback matrix \mathbf{F} such that the closed loop system's poles can be placed in desired locations.*

Meaning that $(\mathbf{A} - \mathbf{BF}) \in \Lambda_d$

This theorem is proven by the fact that the closed loop pole locations are not affected by a change in basis in the state space and in the input space. The state matrix of the transformed system has the same eigenvalues as the original state space matrix.

Proof. Let $\mathbf{x}_c(t) = \mathbf{T}\mathbf{x}(t)$, $\mathbf{u}_c(t) = \mathbf{M}\mathbf{u}(t)$. It follows that

$$\begin{aligned}
\dot{\mathbf{x}}_c &= \mathbf{T}\dot{\mathbf{x}}(t) \\
\dot{\mathbf{x}}_c &= \mathbf{T}(\mathbf{A}\mathbf{x}(t) + \mathbf{B}\mathbf{u}(t)) \\
\dot{\mathbf{x}}_c &= \mathbf{T}\mathbf{A}\mathbf{T}^{-1}\mathbf{x}_c(t) + \mathbf{T}\mathbf{B}\mathbf{M}^{-1}\mathbf{u}_c(t) \\
\dot{\mathbf{x}}_c &= \mathbf{T}\mathbf{A}\mathbf{T}^{-1}\mathbf{x}_c(t) + \mathbf{T}\mathbf{B}\mathbf{M}^{-1}\mathbf{M}\mathbf{u}(t)
\end{aligned}$$

Since the control law is $\mathbf{u}(t) = -\mathbf{F}\mathbf{x}(t)$ (4.20)

$$\begin{aligned}
\dot{\mathbf{x}}_c &= \mathbf{T}\mathbf{A}\mathbf{T}^{-1}\mathbf{x}_c(t) + \mathbf{T}\mathbf{B}\mathbf{M}^{-1}\mathbf{M}(-\mathbf{F}\mathbf{x}(t)) \\
\dot{\mathbf{x}}_c &= \mathbf{T}\mathbf{A}\mathbf{T}^{-1}\mathbf{x}_c(t) - \mathbf{T}\mathbf{B}\mathbf{M}^{-1}\mathbf{M}\mathbf{F}\mathbf{T}^{-1}\mathbf{x}_c(t)
\end{aligned}$$

$$\dot{\mathbf{x}}_c = \mathbf{T}(\mathbf{A} - \mathbf{B}\mathbf{F})\mathbf{T}^{-1}\mathbf{x}_c(t) \quad (4.21)$$

The state matrix of the closed loop system in equation (4.18) is similar to the state matrix of the transformed system of equation (4.21). This proves that a change of basis in the state space and input matrices creates a transformed system that has the same eigenvalues as the original closed loop system where upon viewing equation (4.20)

$$\mathbf{A}_c = \mathbf{T}\mathbf{A}\mathbf{T}^{-1}, \quad \mathbf{B}_c = \mathbf{T}\mathbf{B}, \quad \mathbf{F}_c = \mathbf{F}\mathbf{T}^{-1} \quad (4.22)$$

Here \mathbf{A}_c represents the transformed state matrix, \mathbf{B}_c is the transformed input matrix and \mathbf{F}_c is the transformed state feedback matrix. The M16 is a Single Input Single Output (SISO) System, with the actuator force $F_p(t)$ as the input and the barrel angle $\theta(t)$ as the output. Therefore the SISO format for calculating the state feedback matrix using a change of basis is used to calculate the state feedback matrix \mathbf{F} .

Before designing the state feedback matrix, controllability of the system has to be checked first. The system is controllable if and only if

$$\text{Rank}[\mathbf{B}, \mathbf{AB}, \dots, \mathbf{A}^{n-1}\mathbf{B}] = n \quad (4.23)$$

where n represents the number of states in the state matrix of the nominal plant. If equation (4.23) is satisfied, the system is controllable and can be transformed into controllable canonical form

$$\dot{\mathbf{x}}_c(t) = \mathbf{A}_c \mathbf{x}(t) + \mathbf{B}_c u(t) + \mathbf{d}(t) \quad (4.24)$$

The transformation matrix T in Equation (4.20) must be calculated. Let

$$\beta = [\mathbf{B}, \mathbf{AB}, \dots, \mathbf{A}^{n-1}\mathbf{B}] \quad (4.25)$$

Since it has already been shown that β is controllable, β^{-1} exists

$$\beta^{-1} = \begin{bmatrix} \mathbf{X} \\ \mathbf{q}^T \end{bmatrix} \quad (4.26)$$

where \mathbf{q}^T is the last row of β^{-1} . After solving for the change of basis, the transformation matrix \mathbf{T} is

$$\mathbf{T} = \begin{bmatrix} \mathbf{q}^T \\ \mathbf{q}^T \mathbf{A} \\ \vdots \\ \mathbf{q}^T \mathbf{A}^{n-1} \end{bmatrix} \quad (4.27)$$

The state and input matrices take on the form of

$$\dot{\mathbf{x}}_c(t) = \begin{bmatrix} 0 & 1 & 0 & \cdots & 0 \\ & 0 & \ddots & & \vdots \\ \vdots & \vdots & & & 0 \\ 0 & 0 & & & 1 \\ -a_0 & -a_1 & \cdots & & -a_{n-1} \end{bmatrix} \mathbf{x}_c(t) + \begin{bmatrix} 0 \\ 0 \\ \vdots \\ 0 \\ 1 \end{bmatrix} u(t) \quad (4.28)$$

where the characteristic polynomial of equation (4.28) is

$$\det(sI - A) = s^n + a_{n-1}s^{n-1} + \dots + a_0 \quad (4.29)$$

The characteristic polynomial for equation (4.28) is the same as the characteristic polynomial equation for equation (4.16) therefore both equations have the same eigenvalues. This is proven using Theorem 4.1. After adding a state feedback matrix \mathbf{F}_c to equation (4.24) the new control law is $\mathbf{u}(t) = -\mathbf{F}_c \mathbf{x}(t)$ and the new transformed state equation is

$$\dot{\mathbf{x}}_c(t) = (\mathbf{A}_c - \mathbf{B}_c \mathbf{F}_c) \mathbf{x}(t) + \mathbf{d}(t) \quad (4.30)$$

Equation (4.20) can be written in state space form as

$$\dot{\mathbf{x}}_c(t) = \begin{bmatrix} 0 & 1 & 0 & \cdots & 0 \\ & 0 & \ddots & & \vdots \\ \vdots & \vdots & & 0 & \\ 0 & 0 & & & 1 \\ -a_0 & -a_1 & \cdots & & -a_{n-1} \end{bmatrix} \mathbf{x}_c(t) + \begin{bmatrix} 0 \\ 0 \\ \vdots \\ 0 \\ 1 \end{bmatrix} [-f_{c,0} \quad -f_{c,1} \quad \cdots \quad -f_{c,n-2} \quad -f_{c,n-1}] \mathbf{x}_c(t) \quad (4.31)$$

$$\dot{\mathbf{x}}_c(t) = \begin{bmatrix} 0 & 1 & 0 & \cdots & 0 \\ & 0 & \ddots & & \vdots \\ \vdots & \vdots & & 0 & \\ 0 & 0 & & & 1 \\ -(a_0 + f_{c,0}) & -(a_1 + f_{c,1}) & \cdots & & -(a_{n-1} + f_{c,n-1}) \end{bmatrix} \mathbf{x}_c(t)$$

For equation (4.31) the characteristic polynomial equation for the transformed closed loop system is

$$p_{cl} = s^n + (a_{n-1} + f_{c,n-1})s^{n-1} + (a_{n-2} + f_{c,n-2})s^{n-2} + \dots + (a_0 + f_{c,0}) \quad (4.32)$$

Equation (4.32) allows for the elements of the feedback matrix \mathbf{F}_c to be calculated. This is done by comparing equations (4.19) and (4.32). Equations (4.19) and (4.32) can be set equal to each other by choosing

$$a_{di} = a_i + f_{ci}, \text{ or } f_{ci} = a_{di} - a_i \quad i = 0, 1, \dots, n-1 \quad (4.33)$$

This step creates the state feedback matrix gain \mathbf{F}_c which will place the poles of the transformed closed loop system in their desired location. The state feedback matrix gain \mathbf{F} ,

of the original system is

$$\mathbf{F} = \mathbf{F}_c \mathbf{T} \quad (4.34)$$

Implementing \mathbf{F} into the feedback control system of the original system as shown in Figure 4.7, should increase the performance characteristics of the M16's dynamic stabilizing system. These characteristics include stability, transient response, and steady state error. If the designed \mathbf{F} produces poor results, a new \mathbf{F} is computed and simulated until the feedback control system improves the performance of the M16, meeting the designer's criteria.

4.4 Observer Design

The feedback gain matrix applies a gain to the states of the system, to help produce a desired control signal. However use of a state feedback matrix in simulations assumes that all states of the system can be measured at all times $t \geq t_o$. In reality this is not always possible. Often only the system's produced output can be measured when a system is operating in a real world environment. This results in the task of observing the states' behavior without being able to directly measure the states' values.

An observer can calculate estimated state values $\hat{\mathbf{x}}(t)$ using the control input $\mathbf{u}(t)$, and the output $\mathbf{y}(t)$ of the system. The equation of the observer is

$$\begin{aligned}
 \dot{\hat{\mathbf{x}}}(t) &= \mathbf{A}\hat{\mathbf{x}}(t) + \mathbf{B}\mathbf{u}(t) + \mathbf{G}[\mathbf{y}(t) - \hat{\mathbf{y}}(t)] \\
 \hat{\mathbf{y}}(t) &= \mathbf{C}\hat{\mathbf{x}}(t) \\
 \mathbf{u}(t) &= -\mathbf{F}\hat{\mathbf{x}}(t)
 \end{aligned}
 \tag{4.35}$$

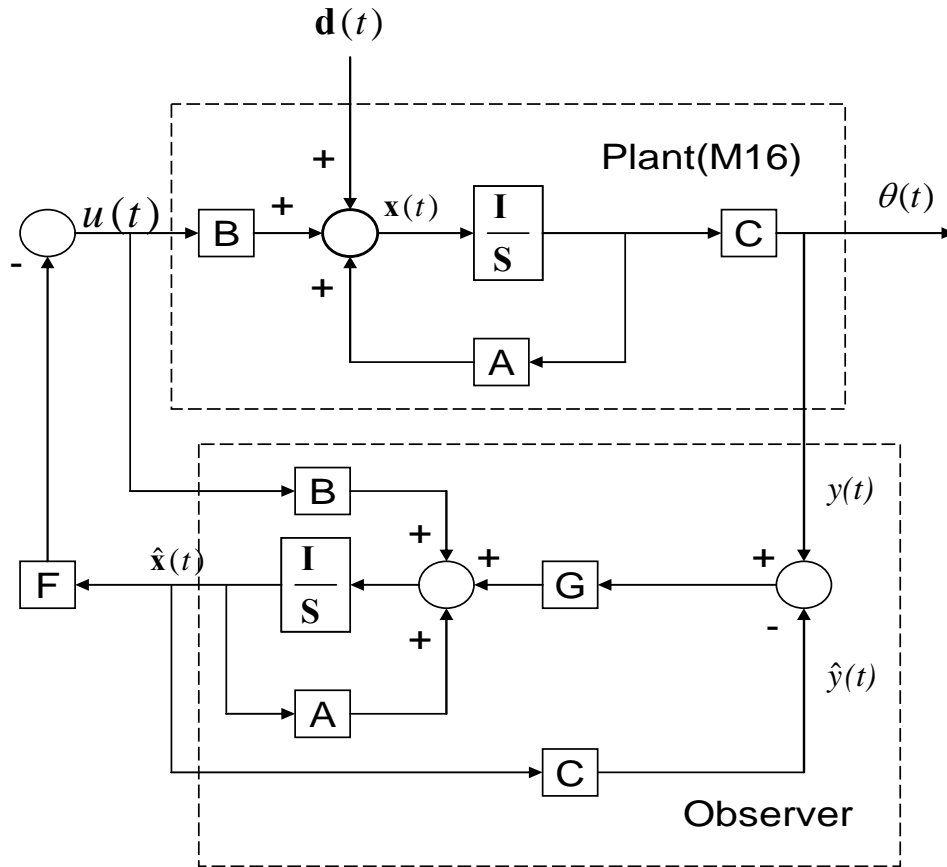


Figure 4.8: Plant with observer connected to the state feedback matrix

The closed loop equation for the system in Figure 4.8 is

$$\begin{bmatrix} \dot{\mathbf{x}}_{plant}(t) \\ \dot{\hat{\mathbf{x}}}(t) \end{bmatrix} = \begin{bmatrix} \mathbf{A} & -\mathbf{BF} \\ \mathbf{GC} & \mathbf{A} - \mathbf{GC} - \mathbf{BF} \end{bmatrix} \begin{bmatrix} \mathbf{x}_{plant}(t) \\ \hat{\mathbf{x}}(t) \end{bmatrix} + \mathbf{d}(t) \quad (4.36)$$

$$\mathbf{y}(t) = [\mathbf{C} \quad \mathbf{0}] \begin{bmatrix} \mathbf{x}_{plant}(t) \\ \hat{\mathbf{x}}(t) \end{bmatrix}$$

Let

$$\mathbf{T} = \begin{bmatrix} \mathbf{I} & \mathbf{O} \\ -\mathbf{I} & \mathbf{I} \end{bmatrix} \quad (4.37)$$

Introducing a change of basis to the state space of equation (4.36) using equation (4.37)

$$\mathbf{T}\mathbf{x}(t) = \begin{bmatrix} \mathbf{I} & \mathbf{O} \\ -\mathbf{I} & \mathbf{I} \end{bmatrix} \begin{bmatrix} \mathbf{x}_{plant}(t) \\ \hat{\mathbf{x}}(t) \end{bmatrix} = \begin{bmatrix} \mathbf{x}_{plant}(t) \\ \hat{\mathbf{x}}(t) - \mathbf{x}(t)_{plant} \end{bmatrix} \quad (4.38)$$

where $\mathbf{x}(t) = \begin{bmatrix} \mathbf{x}_{plant}(t) \\ \hat{\mathbf{x}}(t) \end{bmatrix}$. The transformed state vector in equation (4.38) can be re-written

as

$$\mathbf{x}_T = \begin{bmatrix} \mathbf{x}_{plant}(t) \\ \mathbf{e}(t) \end{bmatrix} \quad (4.39)$$

In equation (4.39) the error vector $\mathbf{e}(t)$ is the calculated difference between the observer's estimated state values $\hat{\mathbf{x}}(t)$ and the true state values of the system $\mathbf{x}(t)$.

The transformed system of equation (4.36) obtained from a change of basis is as follows:

$$\begin{aligned}
 \mathbf{x}_T &= \mathbf{T}\mathbf{x}(t) \\
 \dot{\mathbf{x}}_T &= \mathbf{T}\dot{\mathbf{x}}(t) \\
 \dot{\mathbf{x}}_T &= \mathbf{T} \begin{bmatrix} \mathbf{A} & -\mathbf{BF} \\ \mathbf{GC} & \mathbf{A} - \mathbf{GC} - \mathbf{BF} \end{bmatrix} \begin{bmatrix} \mathbf{x}_{plant}(t) \\ \hat{\mathbf{x}}(t) \end{bmatrix} + \mathbf{d}(t) \\
 \dot{\mathbf{x}}_T &= \mathbf{T} \begin{bmatrix} \mathbf{A} & -\mathbf{BF} \\ \mathbf{GC} & \mathbf{A} - \mathbf{GC} - \mathbf{BF} \end{bmatrix} \mathbf{T}^{-1} \mathbf{x}_T(t) + \mathbf{d}(t) \\
 \dot{\mathbf{x}}_T &= \mathbf{T} \begin{bmatrix} \mathbf{A} & -\mathbf{BF} \\ \mathbf{GC} & \mathbf{A} - \mathbf{GC} - \mathbf{BF} \end{bmatrix} \mathbf{T}^{-1} \begin{bmatrix} \mathbf{x}_{plant}(t) \\ \mathbf{e}(t) \end{bmatrix} + \mathbf{d}(t) \\
 \dot{\mathbf{x}}_T &= \begin{bmatrix} \mathbf{A} - \mathbf{BF} & -\mathbf{BF} \\ \mathbf{0} & \mathbf{A} - \mathbf{GC} \end{bmatrix} \begin{bmatrix} \mathbf{x}_{plant}(t) \\ \mathbf{e}(t) \end{bmatrix} + \mathbf{d}(t) \\
 \begin{bmatrix} \dot{\mathbf{x}}_{plant} \\ \dot{\mathbf{e}}(t) \end{bmatrix} &= \begin{bmatrix} \mathbf{A} - \mathbf{BF} & -\mathbf{BF} \\ \mathbf{0} & \mathbf{A} - \mathbf{GC} \end{bmatrix} \begin{bmatrix} \mathbf{x}_{plant}(t) \\ \mathbf{e}(t) \end{bmatrix} + \mathbf{d}(t)
 \end{aligned} \tag{4.40}$$

In equation (4.40) the eigenvalues of the closed loop system are

$$\lambda(\mathbf{A} - \mathbf{BF}) \cup \lambda(\mathbf{A} - \mathbf{GC}) \tag{4.41}$$

The state matrix of the transformed closed loop system in equation (4.40) is similar to the state matrix of the closed loop system in equation (4.36), meaning it has been shown they both have the same eigenvalues. Equation (4.40) shows that the poles of the plant are the

poles placed by the state feedback irrespective of the observer, and the poles of the controller are the poles placed by observer irrespective of the plant. This is the separation principle.

The separation principle states that the poles of the entire closed loop system is the combination of the poles of the plant placed by the state feedback and the poles added to the system by the observer. This allows for the state feedback matrix gain \mathbf{F} and the observer gain \mathbf{G} to be designed separately. The closed loop form of equation (4.40) can be written as

$$\dot{\mathbf{x}}(t) = (\mathbf{A} - \mathbf{BF})\mathbf{x}(t) - \mathbf{BF}\mathbf{e}(t) + \mathbf{d}(t) \quad (4.42)$$

where

$$\dot{\mathbf{e}}(t) = (\mathbf{A} - \mathbf{GC})\mathbf{e}(t) \quad (4.43)$$

The faster an observer is able to accurately measure the true state values $\mathbf{x}(t)$, the faster the error $\mathbf{e}(t)$ approaches 0. When $\mathbf{e}(t)$ approaches a value of 0, equation (4.42) takes the form of equation (4.18). Accurately estimating the states of a system in a short amount of time will result in a controller that accurately estimates the states' values while allowing the state feedback matrix to remove the disturbances reflected upon the system

After the state feedback matrix gain \mathbf{F} and the observer gain matrix \mathbf{G} have been designed, the observer and the state feedback gain system can be joined together forming one control system to be added to the plant (the original M16 dynamic system). A

successful design of the matrix gains \mathbf{F} and \mathbf{G} results in a stable system, where the states are accurately measured and the outside disturbance affects are minimized.

Before designing an observer, observability of equation (4.1) must first be checked. A system must be observable in order to design an observer for the system.

Definition: The state values in equation (4.1) are observable at time t_0 if for any state $x_0(t_0) \in X$ there exist a finite time t_1 , $t_1 > t_0$ such that knowledge of $\mathbf{y}(t)$ and $\mathbf{u}(t)$, $t_0 \leq t \leq t_1$ suffices to determine $x_0(t_0)$ uniquely. A system is observable if and only if

$$\text{rank} \begin{bmatrix} \mathbf{C} \\ \mathbf{CA} \\ \vdots \\ \mathbf{CA}^{n-1} \end{bmatrix} = n \quad (4.44)$$

where n is the number of states of the system.

To prevent the error dynamics of the observer from having an undesirable affect on the plant, $\mathbf{e}(t)$ must converge to 0 in a shorter time period than the plant's dynamics. The desired time of convergence can be achieved by placing the observer's pole locations $\lambda(\mathbf{A} - \mathbf{GC})$, further in the left half plane of the $j\omega$ -axis than the closed loop plant pole locations $\lambda(\mathbf{A} - \mathbf{BF})$. The observer's poles are generally placed 3-10 times further to the left in respect to the location of the plant's closed loop poles.

After the observer's desired pole locations have been chosen, the next step is to design the observer's gain matrix \mathbf{G} of the observer. This process is very similar to constructing the state feedback gain matrix \mathbf{F} . Therefore using the form of equation (4.41),

$$\lambda(\mathbf{A} - \mathbf{GC}) = \lambda(\mathbf{A}^T - \mathbf{C}^T \mathbf{G}^T) \quad (4.45)$$

From equation (4.45) the observer gain \mathbf{G} can be calculated when $(\mathbf{A}^T, \mathbf{C}^T)$ is controllable. As has been shown, the form used in placing $(\mathbf{A} - \mathbf{BF})$ in controllable canonical form to solve for \mathbf{F} , can be used to place $(\mathbf{A}^T - \mathbf{C}^T \mathbf{G}^T)$ in controllable canonical form to solve for \mathbf{G} .

After adding an observer to the system it may be observed that the observer amplifies the disturbance signal. An amplified disturbance signal is an undesirable performance characteristic of some observers. However the disturbance may be mitigated by adjusting the observer's pole locations and re-calculating a new corresponding gain matrix \mathbf{G} , respectively,, until the closed loop control system meets the designer's specifications.

4.5 LQG

It is important that the control system designed to stabilize the M16 rifle meet all design criteria. The fact that the stabilizing system must produce an acceptable output while estimating and controlling the states' values, along with the fact that the control input of the system requires a system of weights to regulate these performance aspects of the system led to the decision to develop a Linear Quadratic Gaussian (LQG) controller.

The linear quadratic regulator is used to minimize the performance measure

$$J = \int_{t_0}^{t_f} \mathbf{x}^T(t) \mathbf{Q} \mathbf{x}(t) + \mathbf{u}^T \mathbf{R} \mathbf{u}(t) dt \quad (4.46)$$

where \mathbf{Q} is a symmetric, positive semi-definite matrix, and \mathbf{R} is a symmetric, positive definite matrix. The \mathbf{Q} matrix is a symmetric positive semi-definite matrix to ensure that the cost function J is convex with a local minimum. \mathbf{R} is a symmetric positive definite matrix to ensure that the weighting coefficients for the optimal control $\mathbf{u}(t)$ are not equal to 0. This guarantees that $\mathbf{u}(t) \neq 0$. A control input $\mathbf{u}(t) = 0$ will allow the state variables $\mathbf{x}(t)$ to approach ∞ , which is an undesirable performance characteristic of the system.

Since the \mathbf{Q} matrix is positive semi-definite matrix all of its diagonal elements are non-negative. These diagonal elements q_{ii} are weights that have an affect on the corresponding system state variables $x_i(t)$. Increasing these weights places a larger penalty on the deviation of $x_i(t_f)$ in relation to $x_i(t_0)$. A weight value of $q_{ii} = 0$ means that the final value of $x_i(t)$ is of no concern.

The diagonal elements of \mathbf{R} are non-negative as well. The diagonal elements of \mathbf{R} , r_{ii} are weights that have an affect on the corresponding control values $u_i(t)$. Increasing the weights of \mathbf{R} reduces the amount of control expenditure $\mathbf{u}(t)$.

Since the control system for the M16 model is linear time invariant, the ratio between the weight values of \mathbf{Q} and \mathbf{R} are of importance. Different weight values for \mathbf{Q} and \mathbf{R} with the same ratio have the same effect on the control system. Using the weight values of \mathbf{Q} and \mathbf{R} and their ratio, the LQR produces an optimal feedback

matrix. This optimal feedback matrix produces the optimal control system input $\mathbf{u}(t)$ in relation to the designer's desired state values and the desired control expenditure.

A similar process is carried out to design the optimal gain \mathbf{G} for the observer.

The performance measure of the observer is

$$J = \int_{t_0}^{t_f} \hat{\mathbf{x}}^T(t) \mathbf{Q} \hat{\mathbf{x}}(t) + \mathbf{y}(t)^T \mathbf{R} \mathbf{y}(t) dt \quad (4.47)$$

The observer for this M16 system is linear time invariant, therefore the ratio of weight values between \mathbf{Q} and \mathbf{R} has an effect on the performance of the observer.

The closed loop equation for the M16 stabilizing control system is

$$\dot{\mathbf{x}}(t) = (\mathbf{A} - \mathbf{B}\mathbf{F})\mathbf{x}(t) - \mathbf{B}\mathbf{F}\mathbf{e}(t) + \mathbf{d}(t) \quad (4.48)$$

The motivation behind using a linear quadratic regulator to design the optimal gain \mathbf{G} comes from equation (4.48). An optimal gain \mathbf{G} minimizes the error variance between the observer's estimated states $\hat{\mathbf{x}}(t)$ and the plant's actual states $\mathbf{x}(t)$. Providing accurately measured state values of the system to the optimal feedback matrix allows the feedback matrix to calculate a superior system control input to reduce the effects of disturbances on the system's performance.

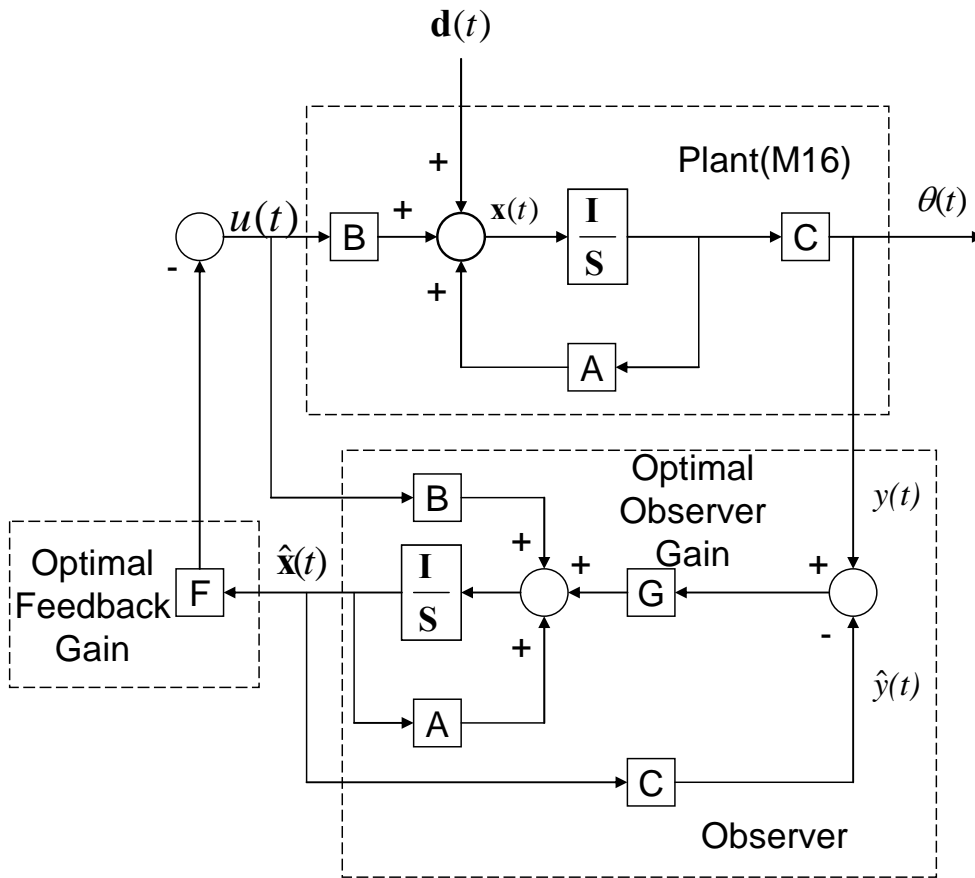


Figure 4.9 LQG system with optimal feedback gain and optimal observer gain

Chapter 5

Numerical Models

This chapter is a layout of the numerical models of the plant and the controllers developed in this paper using the theory from Chapter 4. Pole locations for each controller are presented to certify that all control systems are stable before their use in simulations.

5.1 Uncontrolled System

The uncontrolled M16 system is a linear time-invariant system whose state equation is written as

$$\begin{aligned}\dot{\mathbf{x}}(t) &= \mathbf{Ax}(t) + \mathbf{Bu}(t) + \mathbf{d}(t) \\ \mathbf{y}(t) &= \mathbf{Cx}(t)\end{aligned}\tag{5.1}$$

The numerical model of equation (5.1) is

$$\begin{aligned}\begin{bmatrix} \dot{x}_1(t) \\ \dot{x}_2(t) \\ \dot{y}_1(t) \\ \dot{y}_2(t) \end{bmatrix} &= \begin{bmatrix} 0 & 1 & 0 & 0 \\ -48408 & -345.79 & 16609 & 231.68 \\ 0 & 0 & 0 & 1 \\ -1395 & 0 & 0 & 0 \end{bmatrix} \begin{bmatrix} x_1(t) \\ x_2(t) \\ y_1(t) \\ y_2(t) \end{bmatrix} + \\ &\begin{bmatrix} 0 \\ 0.19783 \\ 0 \\ 0.32367 \end{bmatrix} F_p(t) + \begin{bmatrix} 0 \\ 5.0111\sin(\omega t) + 0.77565\cos(\omega t) \\ 0 \\ 0.00318\sin(\omega t) \end{bmatrix}\end{aligned}\tag{5.2}$$

$$\theta(t) = [0010] \begin{bmatrix} x_1(t) \\ x_2(t) \\ y_1(t) \\ y_2(t) \end{bmatrix}$$

The transfer function of the system is

$$H(s) = \frac{0.3237s^2 + 111.9s + 15390}{s^4 + 345.8s^3 + 48410s^2 + 323200s + 2.317 * 10^7} \quad (5.3)$$

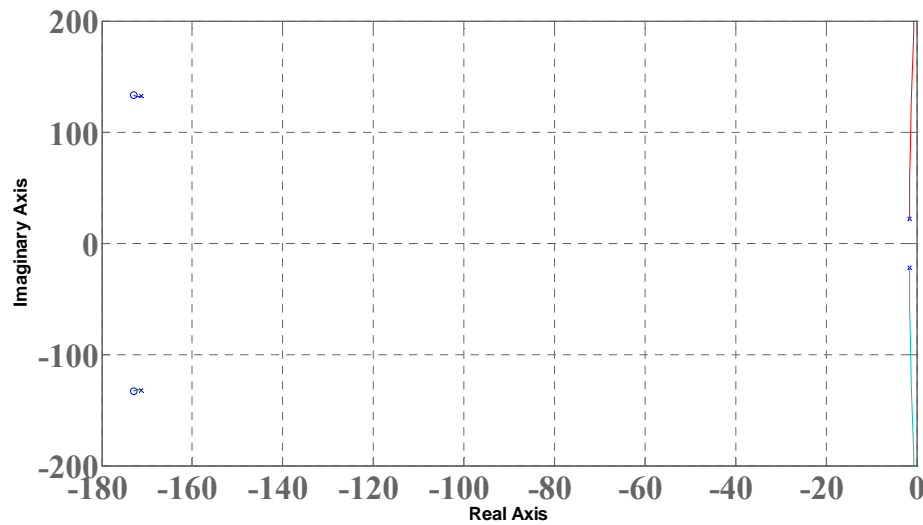


Figure 5.1: Root locus of the uncontrolled system

The root locus of the uncontrolled system as shown in Figure 5.1, shows that the system is a marginally stable fourth order system. It has two dominant open loop complex poles

near the $j\omega$ -axis. The remaining two open loop poles of the system are complex poles and are located substantially further to the left of the $j\omega$ - axis than the dominant open loop poles.

Table 5.1 Open Loop Pole Location

Pole 1	-1.6413 +22.193i
Pole 2	-1.6413 -22.193i
Pole 3	-171.25 +132.14i
Pole 4	-171.25 -132.14i

5.2 Unity Feedback

The unity feedback controller has a numerical model very similar to the uncontrolled system. It's transfer function

$H(s) = \frac{0.3237s^2 + 111.9s + 153900}{s^4 + 345.8s^3 + 48410s^2 + 323300s + 2.319 * 10^7}$	(5.4)
---	-------

which is very similar to the transfer function of the uncontrolled system in equation (5.3).

The root locus for the unity feedback system is

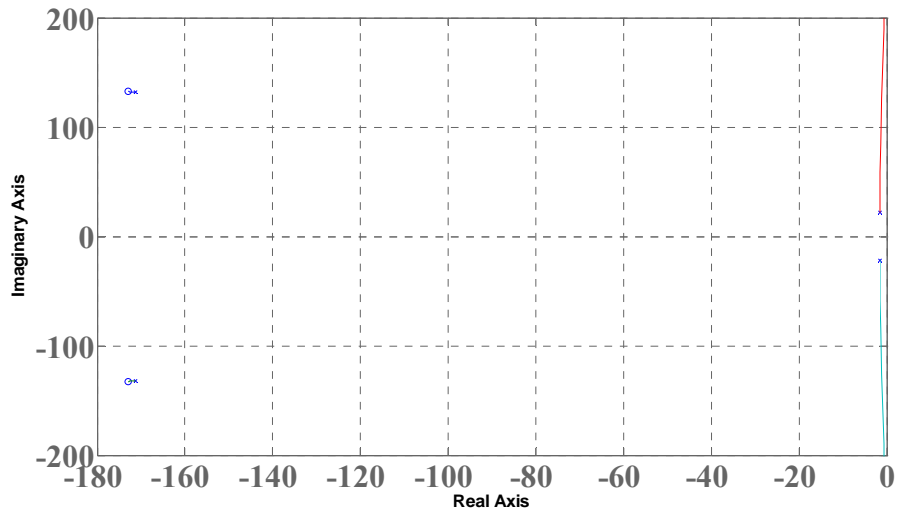


Figure 5.2: Root locus of the plant connected to unity feedback system

In Table 5.2 are the open loop pole locations for the unity feedback controller system.

Table 5.2 Open loop pole locations

Pole 1	$-1.6413 + 22.2i$
Pole 2	$-1.6413 - 22.2i$
Pole 3	$-171.25 + 132.14i$
Pole 4	$-171.25 - 132.14i$

5.3 Compensator Design

The compensator for the M16 control system is designed using the root locus of the uncontrolled system from Figure 5.1. The departure angle for the complex Pole 1 located at $-1.6413 + 22.193i$ is calculated using equation (5.5)

$$\sum \angle zeros - \sum \angle poles = 180^\circ \quad (5.5)$$

After choosing a point that is a short distance ε away from Pole 1, equation (5.5) when applied to the M16 system takes the form of

$$42^\circ + 33^\circ - 33^\circ - 42^\circ - 90^\circ - \theta_{Pole1} = 180^\circ \quad (5.6)$$

$$\theta_{Pole1} = -270^\circ = 90^\circ \quad (5.7)$$

$$\phi_{di} - \phi_i = \arg(C(j\omega_i)) \quad (5.8)$$

Equation (5.7) is the departure angle of Pole 1. Using the fact that the real part of Pole 1 is small equation (5.8) states that the phase of the compensator $C(j\omega_1)$, placed at the

resonant frequency of Pole 1 can be used to determine the departure angle of Pole 1. The phase of $C(j\omega_i)$ can be calculated by subtracting the pole departure angle ϕ_i , from the desired pole departure angle ϕ_d . Where i represents a particular pole and ω_i represents the corresponding resonant frequency of the i^{th} pole. For the M16 system considered, problem $\phi_{di} = 180^\circ$, $\phi_i = 90^\circ$, and $\omega_i = 22.193 \text{ rad/s}$. After substituting equation (5.7) into equation (5.8) and plugging in $\phi_{di} = 180^\circ$, the phase of the designed compensator can be solved for.

$$\arg(C(j22.193 \text{ rad/s})) = 180^\circ - 90^\circ = 90^\circ \quad (5.9)$$

A positive angle for equation (5.9) means that a lead compensator may be used to add phase to the original uncontrolled system to adjust the departure angle of that particular i^{th} pole. Using equation (5.9), a lead compensator of phase $\arg(C(j22.193 \text{ rad/s})) = 90^\circ$ at $\omega = 22.193 \text{ rad/s}$ should result in the desired departure angle results on the new root locus. Figure 5.3 shows a Bode plot of the designed compensator

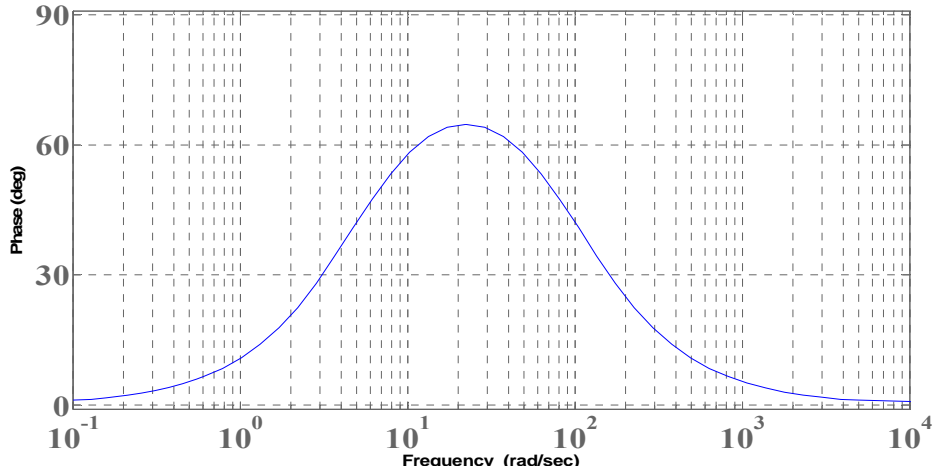


Figure 5.3: Bode plot of the designed lead compensator's phase response

The designed compensator in Figure 5.3 is a lead compensator that has a maximum phase value at 64.8° at $\omega = 22.1 \text{ rad/sec}$. After trying several designs, this compensator provided the optimal results.

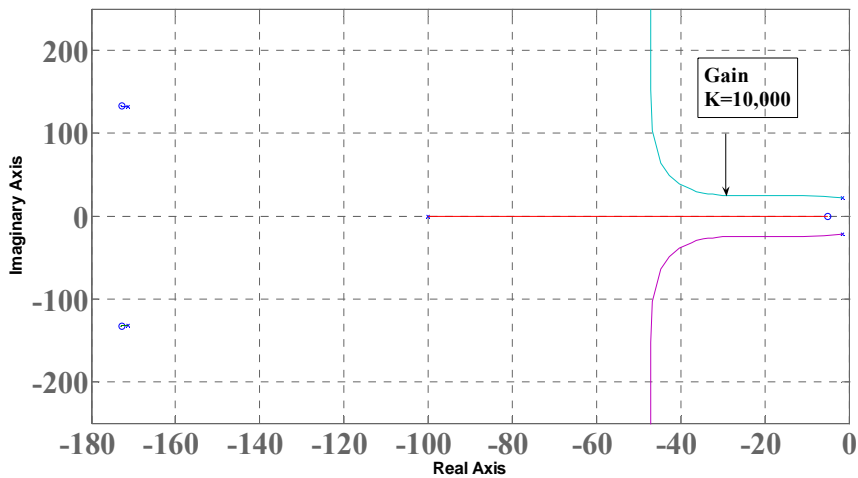


Figure 5.4: Root locus of the compensated original system

The root locus of Figure 5.4 shows how adding the compensator to the system, modified the departure angles of the dominant complex poles of the system. This is a drastic change in departure angle, in comparison to the departure angle in Figure 1. The root locus was used to choose the optimal gain $K = 10,000$ for the compensator. The resulting 180° departure angles of these poles dramatically increases the output performance of the M16 rifle system. In addition to having a reduced barrel targeting error, the system is no longer marginally stable.

Table 5.3 Open loop pole locations

Pole 1	-1.6428+22.193i
Pole 2	-1.6428-22.193i
Pole 3	-171.25+132.14i
Pole 4	-171.25-132.14i
Pole 5	-99.997

5.4 State Feedback Matrix

Controllability of the system must be checked before the state feedback matrix can be designed. Equation (5.10) has full rank therefore the system is controllable.

$$\text{Rank}[\mathbf{B}, \mathbf{AB}, \mathbf{A}^2\mathbf{B}, \mathbf{A}^3\mathbf{B}] = 4 \quad (5.10)$$

Next the transformation matrix \mathbf{T} must be solved for in order to transform the system into controllable canonical form.

$$\mathbf{T} = \begin{bmatrix} 1.451 * 10^{-4} & -2.2943 * 10^{-4} & -2.3937 * 10^{-7} & 1.463 * 10^{-7} \\ -3.9757 * 10^{-3} & 1.1383 * 10^{-2} & -1.4666 * 10^{-4} & 8.964 * 10^{-5} \\ -2.4359 & 6.9746 & 6.2098 * 10^{-2} & -3.7954 * 10^{-2} \\ 1031.4 & -2953.1 & -14.498 & 11.951 \end{bmatrix} \quad (5.11)$$

Equations (5.12) and (5.13) are the \mathbf{A} and \mathbf{B} matrices of the original system transformed into controllable canonical form based on their transformations by the \mathbf{T} matrix.

$$\mathbf{A}_c = \begin{bmatrix} 0 & 1 & 0 & 0 \\ 0 & 0 & 1 & 0 \\ 0 & 0 & 0 & 1 \\ -2.317 * 10^7 & -3.232 * 10^5 & -48408 & -345.79 \end{bmatrix} \quad (5.12)$$

$$\mathbf{B}_c = \begin{bmatrix} 0 \\ 0 \\ 0 \\ 1 \end{bmatrix} \quad (5.13)$$

$$\dot{x}_c(t) = (A_c - B_c F_c)x_c(t)$$

$$= \begin{bmatrix} 0 & 1 & 0 & 0 \\ 0 & 0 & 1 & 0 \\ 0 & 0 & 0 & 1 \\ -2.317 \cdot 10^7 & -3.232 \cdot 10^5 & -48408 & -345.79 \end{bmatrix} x_c(t) - \begin{bmatrix} 0 \\ 0 \\ 0 \\ 1 \end{bmatrix} \begin{bmatrix} f_{c(0)} & f_{c(1)} & f_{c(2)} & f_{c(3)} \end{bmatrix} x_c(t)$$

(5.14)

$$= \begin{bmatrix} 0 & 1 & 0 & 0 \\ 0 & 0 & 1 & 0 \\ 0 & 0 & 0 & 1 \\ \left(-2.317 \cdot 10^7 - f_{c(0)}\right) & \left(-3.232 \cdot 10^5 - f_{c(1)}\right) & \left(-48408 - f_{c(2)}\right) & \left(-345.79 - f_{c(3)}\right) \end{bmatrix} x_c(t)$$

The characteristic polynomial for equation (5.14) is given by

$$s^4 + (345.79 + f_{c(3)})s^3 + (48408 + f_{c(2)})s^2 + (3.232 \cdot 10^5 + f_{c(1)})s + (2.317 \cdot 10^7 + f_{c(0)})$$

(5.15)

The new desired pole locations for the system are

Table 5.4 Desired pole locations placed by state feedback

Pole 1	-200 +0.5i
Pole 2	-200 -0.5i
Pole 3	-400 +0.5i
Pole 4	-400 -0.5i

The characteristic polynomial for the new desired pole locations is

$$s^4 + 1200s^3 + 5.2 * 10^5 s^2 + 9.6 * 10^7 s + 6.4001 * 10^9 \quad (5.16)$$

The elements of the transformed feedback matrix F_c in equation (5.15) can be solved for by substituting the polynomial coefficients of equation (5.15) into the corresponding coefficients of equation (5.16).

$$\begin{aligned} (345.79 + f_{c(3)}) &= 1200 \\ (48408 + f_{c(2)}) &= 5.2 * 10^5 \\ (3.232 * 10^5 + f_{c(1)}) &= 9.6 * 10^7 \\ (2.317 * 10^7 + f_{c(0)}) &= 6.4001 * 10^9 \end{aligned} \quad (5.17)$$

After solving for the elements of the transformed feedback matrix in equation (5.17), the transformed feedback matrix is

$$F_c = [6.3769 * 10^9 \quad 9.5677 * 10^7 \quad 471592 \quad 854.21] \quad (5.18)$$

$$F = F_c T \quad (5.19)$$

Using equation (4.34) the state feedback matrix gain for the original coordinate system is

$$F = [2.7715 * 10^5 \quad 3.9267 * 10^5 \quad 1341.7 \quad 1819.1] \quad (5.20)$$

Matrix F in equation (5.20) is placed in a state feedback loop that is added to the original uncontrolled M16 plant model. Figure 5.5 is the root locus of the original system after the state feedback loop is added to it.

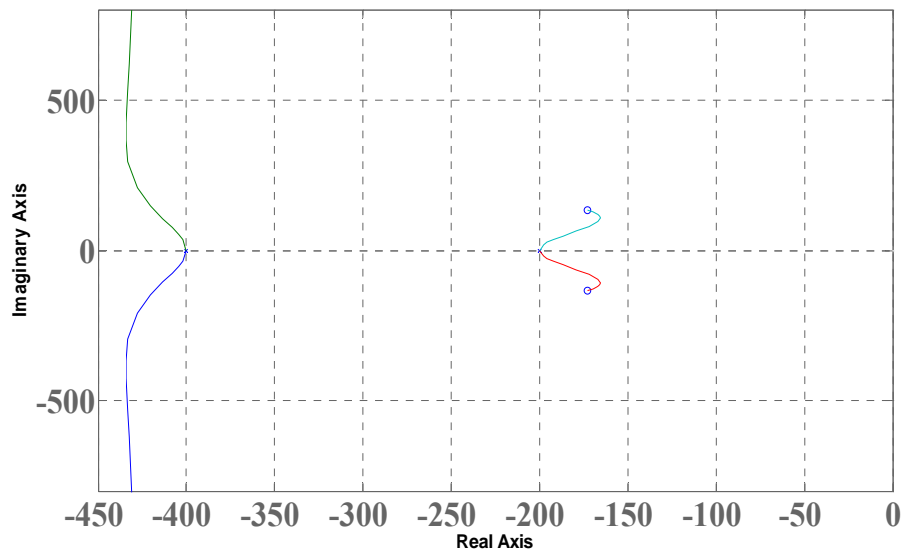


Figure 5.5: Root locus of the system with its poles placed by state feedback

The root locus of the state feedback system in Figure 5.5 shows that all system poles are located in the left half of the complex plane, meaning that the system is stable. Also the state feedback matrix was successful in placing the poles further to the left of the $j\omega$ -axis than they were in the original uncontrolled system. This creates a system that

is stable and very responsive to diminishing the human disturbances induced upon the M16 rifle.

Table 5.5 Actual pole locations place by state feedback

Pole 1	-200+0.5i
Pole 2	-200-0.5i
Pole 3	-400+0.5i
Pole 4	-400-0.5i

5.5 Observer Design

Before designing an observer to estimate the states of the system, the system must be checked for observability. For this particular system equation (5.21) has full rank, therefore the system is observable.

$$\text{Rank} \begin{bmatrix} \mathbf{C} \\ \mathbf{CA} \\ \mathbf{CA}^2 \\ \mathbf{CA}^3 \end{bmatrix} = 4 \quad (5.21)$$

The state feedback matrix gain \mathbf{F} , calculated in the previous section will be used in the observer control system. Using the separation principle, the observer gain \mathbf{G} is calculated to place the poles of the observer four times further to the left of the $j\omega$ -axis in relation to the pole locations of the state feedback system. These pole locations are

Table 5.6 Observer pole locations

Pole 1	-800 + 2i
Pole 2	-800 - 2i
Pole 3	-1600 + 2i
Pole 4	-1600 - 2i

The observer gain matrix \mathbf{G} is calculated in a manner similar to the state feedback matrix \mathbf{F} . The transformation matrix \mathbf{T} is calculated and used to place the system into canonical form.

$$\mathbf{T} = \begin{bmatrix} 0 & 0 & -7.1683 \cdot 10^{-4} & 0 \\ 0 & -7.1683 \cdot 10^{-4} & 0.24787 & 0 \\ 0 & 0.24787 & -51.011 & 1 \\ 1 & -51.011 & 5871.7 & -345.79 \end{bmatrix} \quad (5.22)$$

Equations (5.23) and (5.24) are the \mathbf{A}^T and \mathbf{C}^T matrices in controllable canonical form based on their transformations by the \mathbf{T} matrix.

$$\mathbf{A}^T_c = \begin{bmatrix} 0 & 1 & 0 & 0 \\ 0 & 0 & 1 & 0 \\ 0 & 0 & 0 & 1 \\ -2.317 * 10^7 & -3.232 * 10^5 & -48408 & -345.79 \end{bmatrix} \quad (5.23)$$

$$\mathbf{C}^T_c = \begin{bmatrix} 0 \\ 0 \\ 0 \\ 1 \end{bmatrix} \quad (5.24)$$

$$\mathbf{A}^T_c - \mathbf{C}^T_c \mathbf{G}^T_c = \begin{bmatrix} 0 & 1 & 0 & 0 \\ 0 & 0 & 1 & 0 \\ 0 & 0 & 0 & 1 \\ -2.317 * 10^7 & -3.232 * 10^5 & -48408 & -345.79 \end{bmatrix} - \begin{bmatrix} 0 \\ 0 \\ 0 \\ 1 \end{bmatrix} \begin{bmatrix} g_{c(0)} & g_{c(1)} & g_{c(2)} & g_{c(3)} \end{bmatrix} \quad (5.25)$$

$$= \begin{bmatrix} 0 & 1 & 0 & 0 \\ 0 & 0 & 1 & 0 \\ 0 & 0 & 0 & 1 \\ \left(-2.317 * 10^7 - g_{c(0)}\right) & \left(-3.232 * 10^5 - g_{c(1)}\right) & \left(-48408 - g_{c(2)}\right) & \left(-345.79 - g_{c(3)}\right) \end{bmatrix}$$

The characteristic polynomial for equation (5.25) is

$$s^4 + \left(345.79 + g_{c(3)}\right)s^3 + \left(48408 + g_{c(2)}\right)s^2 + \left(3.232 * 10^5 + g_{c(1)}\right)s + \left(2.317 * 10^7 + g_{c(0)}\right) \quad (5.26)$$

The characteristic polynomial for the new desired pole locations of Table 5.7 is

$$s^4 + 4800s^3 + 8.32 * 10^6 s^2 + 6.144 * 10^9 s + 1.6384 * 10^{12} \quad (5.27)$$

The elements of the transformed observer gain matrix \mathbf{G}^T_c in equation (5.26) can be solved for by substituting the polynomial coefficients of equation (5.26) into the corresponding polynomial coefficients of equation (5.27).

$$\begin{aligned} (345.79 + g_{c(3)}) &= 4800 \\ (48408 + g_{c(2)}) &= 8.32 * 10^6 \\ (3.232 * 10^5 + g_{c(1)}) &= 6.144 * 10^9 \\ (2.317 * 10^7 + g_{c(0)}) &= 1.6384 * 10^{12} \end{aligned} \quad (5.28)$$

After solving for the elements in equation (5.28), the transformed feedback matrix is

$$\mathbf{G}^T_c = \begin{bmatrix} 1.684 * 10^{12} & 6.144 * 10^9 & 8.272 * 10^6 & 4454.21 \end{bmatrix} \quad (5.29)$$

$$\mathbf{G}^T = \mathbf{G}^T_c \mathbf{T} \quad (5.30)$$

After taking the transpose of equation (5.30) the observer gain matrix \mathbf{G} is

$$\mathbf{G} = \begin{bmatrix} 4454.2 \\ -2.581 \cdot 10^6 \\ -4.738 \cdot 10^7 \\ 6.7314 \cdot 10^6 \end{bmatrix} \quad (5.31)$$

Figure 5.6 shows the root locus of the observer gain system with state feedback.

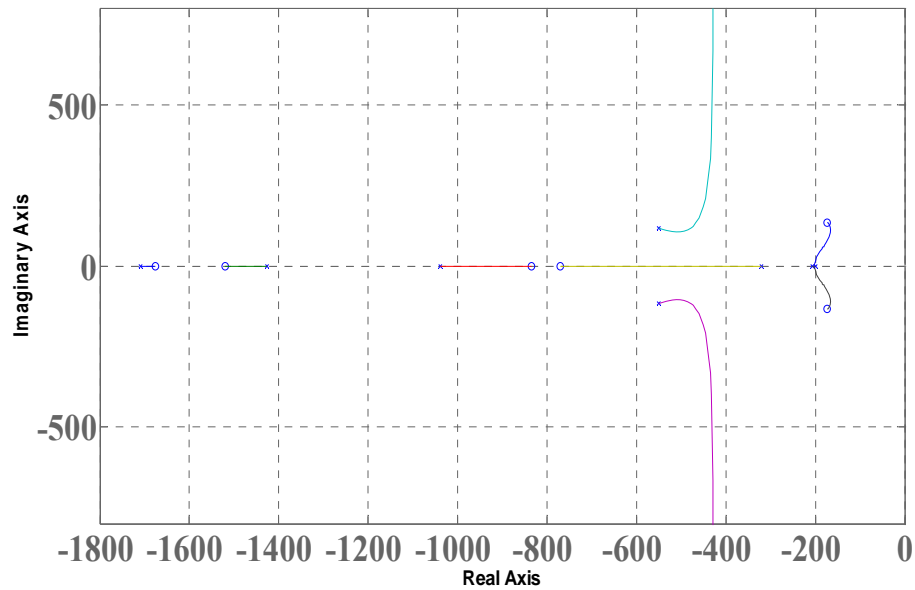


Figure 5.6: Root locus of state feedback system with an observer

The root locus of the observer control system includes the open loop poles placed by the state feedback control system as well as the open loop poles of the observer. All poles are located in the left half plane of the axis, therefore it can be concluded that the system is stable.

Table 5.7 Pole locations of the state feedback with an observer

Pole 1	-200 +0.5i
Pole 2	-200 -0.5i
Pole 3	-400 +0.5i
Pole 4	-400 -0.5i
Pole 5	-800 +2i
Pole 6	-800 -2i
Pole 7	-1600 +2i
Pole 8	-1600 -2i

5.6 Linear Quadratic Gaussian

In the LQG method the state feedback matrix and the observer gain were initially designed separately, leading to undesirable performance marks for the observer and the output targeting error of the system. An alternate method was applied by using the LQG method to design the optimal state feedback matrix and the optimal observer gain together, while both systems are connected to the original plant. Controlling the state values as well as the targeting error of the system is the main factor in deciding the element values of the **Q** matrix for the state feedback matrix. The **R** matrix on the other hand used to design the state feedback matrix is modified to control the magnitude of actuator force. The **Q** and **R** matrixes for the observer gain were designed using similar motivation. However the design for the **Q** and **R** matrices for the observer gain has

emphasis on controlling all of the states of the system in order to produce proper state estimates.

For the state feedback, the \mathbf{Q} and \mathbf{R} matrix combination is

$$\mathbf{Q} = \begin{bmatrix} 1*10^{22} & 0 & 0 & 0 \\ 0 & 1 & 0 & 0 \\ 0 & 0 & 1 & 0 \\ 0 & 0 & 0 & 1*10^{10} \end{bmatrix} \quad (5.32)$$

$$\mathbf{R} = [1]$$

For the observer gain the \mathbf{Q} and \mathbf{R} matrix combination is

$$\mathbf{Q} = \begin{bmatrix} 1*10^{11} & 0 & 0 & 0 \\ 0 & 10 & 0 & 0 \\ 0 & 0 & 10 & 0 \\ 0 & 0 & 0 & 10 \end{bmatrix} \quad (5.33)$$

$$\mathbf{R} = [1]$$

The root locus for the LQG system is show in Figure 5.7.

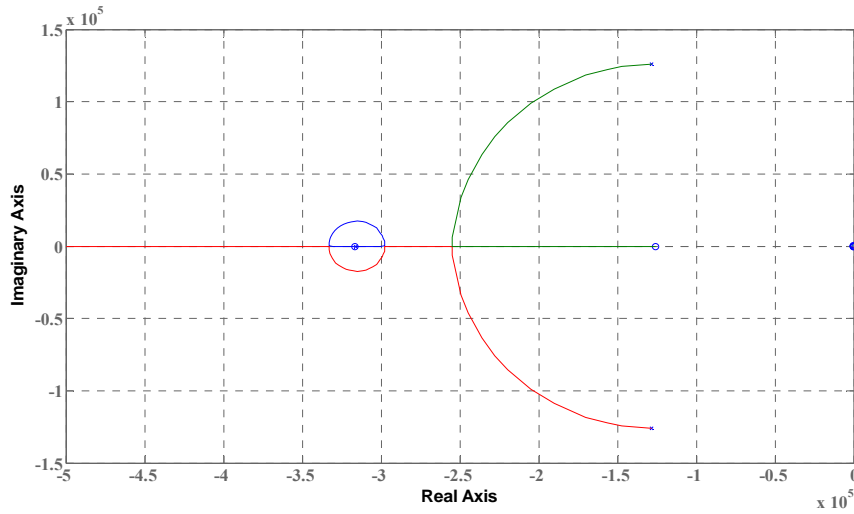


Figure 5.7: Root locus of LQG system

The root locus shows that the LQG system is stable. It includes the poles of the optimal state feedback system along with the optimal observer gain system.

Table 7 Closed Loop Locations

Pole 1	$-3.1623 \cdot 10^5$
Pole 2	$-1.2824 \cdot 10^5 + 1.2618 \cdot 10^5 i$
Pole 3	$-1.2824 \cdot 10^5 - 1.2618 \cdot 10^5 i$
Pole 4	-7.0215
Pole 5	$-172.89 + 132.9i$
Pole 6	$-172.89 - 132.9i$
Pole 7	$-169.38 + 131.68i$
Pole 8	$-169.38 - 131.68i$

Chapter 6

Results

This chapter discusses and presents the simulation results of the designed controlled system. Simulink of Matlab was the software used to create and test all designed control systems. First the plant model for the M16 rifle was designed. The plant model including human induced disturbances was designed in Chapter 2. The disturbances are 3Hz sinusoidal waves with various amplitudes. The amplitudes were modified to result in the allowable plant targeting error of $\theta(t) = 3mrad$, which is equivalent to 3 silhouettes at a distance of $D = 250m$. The value of $\theta(t)$ is calculated using equation (6.1), with the target distribution $s = \pm 0.75m$. Each simulation in this chapter is on a time interval of $0 \leq t \leq 3s$.

$$\theta(t) = \tan^{-1}\left(\frac{s}{D}\right) \quad (6.1)$$

6.1 Uncontrolled System

Figure 6.1 shows the targeting error $\theta(t)$ of the uncontrolled M16 plant model.

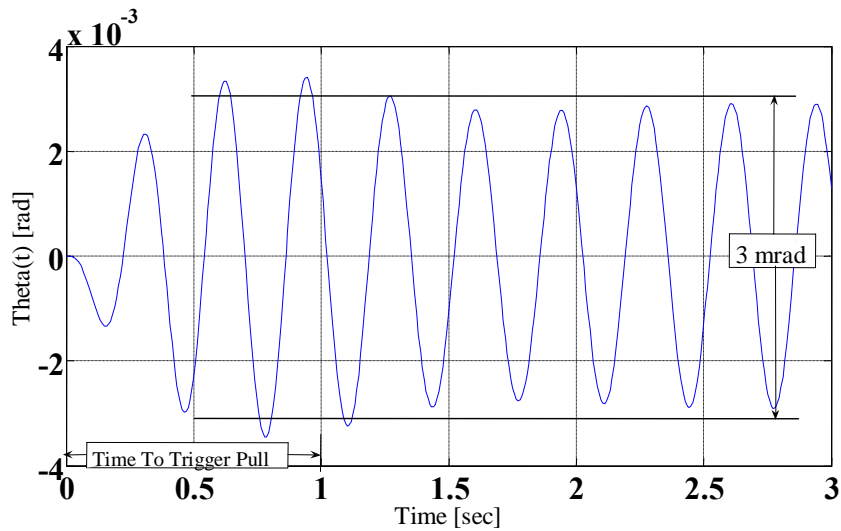


Figure 6.1: Targeting error for uncontrolled system

In Figure 6.1 the M16 plant model along with human disturbances produces a targeting error $\theta(t)$ around 3mrad which is within the limits of the targeting error distribution allowed by the constraint of the actuator displacement magnitude x_p . Figure 6.2 displays the dynamic behavior of $x_p(t)$, for this state value has to be monitored to test if the control design meets specification. The actuator force $F_p(t) = 0$ for the uncontrolled system.

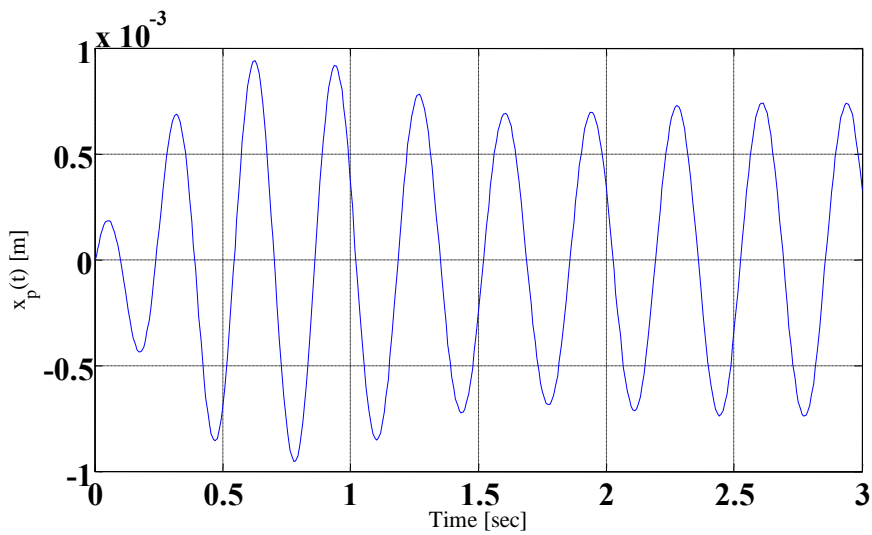


Figure 6.2: Actuator displacement of the uncontrolled system

6.2 Unity Feedback

As stated previously, the system of negative unity feedback is one which the output $\theta(t)$ is fed back into the system. Figure 6.3 shows the output of the unity feedback system versus the output of the uncontrolled system.

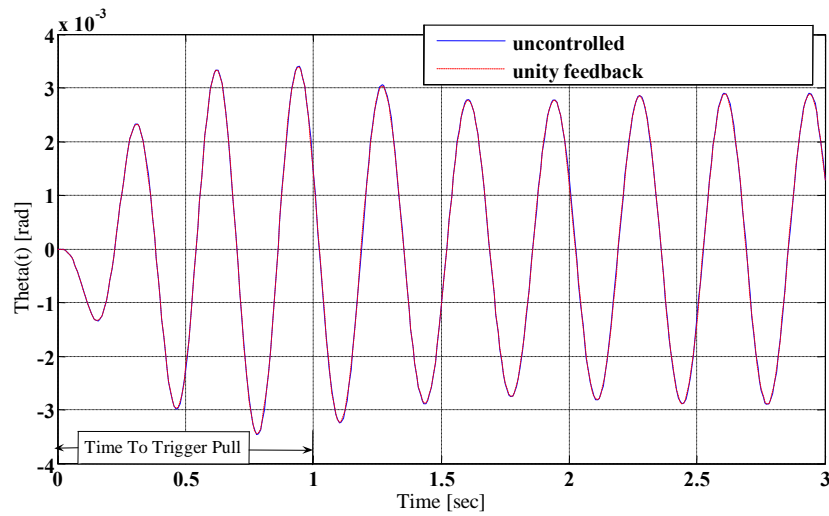


Figure 6.3: Targeting error for uncontrolled system vs. unity feedback system

Observation of Figure 6.3 reveals that the targeting error $\theta(t)$ of both systems is very similar. The uncontrolled output is represented as a solid blue line, while the unity feedback is a dashed red line with “-” point markers.

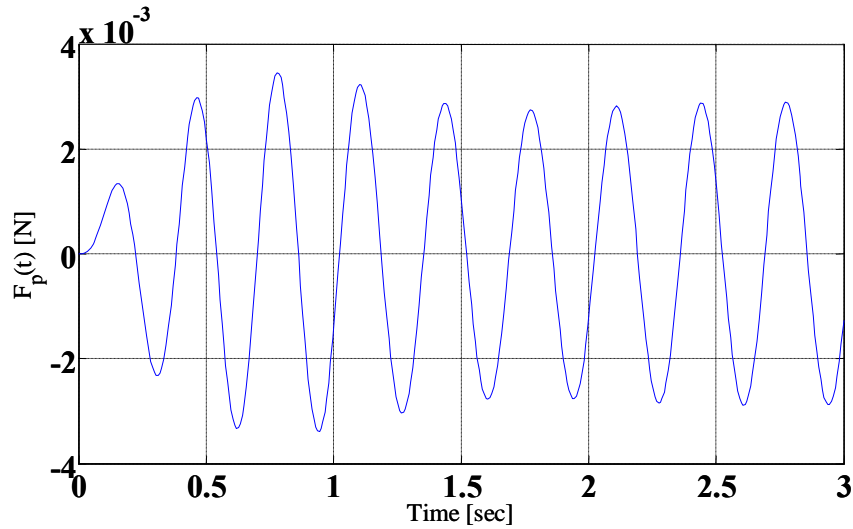


Figure 6.4: Actuator stabilization force of the unity feedback control system

The maximum value of $F_p(t) = 3.5 * 10^{-3} N$, is well below the actuator saturation limit of 8N. For the negative unity feedback system the actuator force expenditure $F_p(t)$ is very low. The actuator displacement $x_p(t)$ meets criteria as show in Figure 6.5.

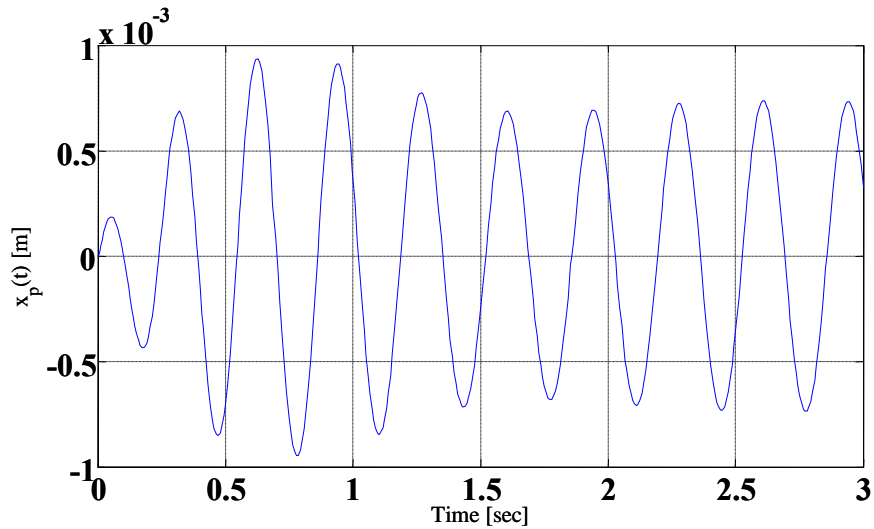


Figure 6.5: Actuator displacement of the unity feedback control system

6.3 Compensator

The next control system applied to the plant is a lead compensator. This control system is added to address the dominant complex poles of the uncontrolled system that are located near the $j\omega$ -axis in order to change the performance of the system from being marginally stable.

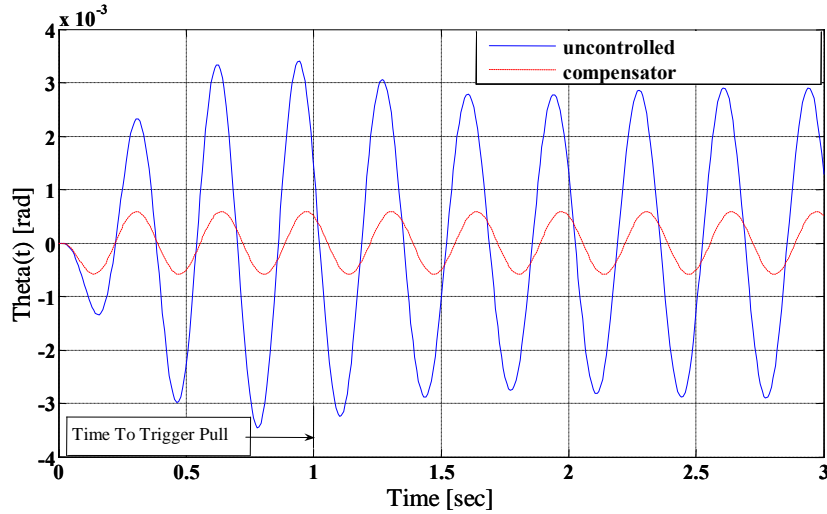


Figure 6.6: Targeting error for uncontrolled system vs. compensated system

The amplitude of the barrel vibration has significantly been decreased as a result of adding a lead compensator control system to the M16. The lead compensator was successful in adding phase to the system which acted as a damper to reduce the jitter resonance in the frequency response. Figure 6.6 shows the output of the compensated system in relation to the original uncontrolled system. The uncontrolled system is graphed as a solid blue line while the compensator controlled system is a dashed red line with “--” point markers. The next parameter’s behavior to observe is the actuator stabilization.

The compensated system meets specification for $F_p(t)$ and $x_p(t)$ as shown in

Figures 6.7 and 6.8.

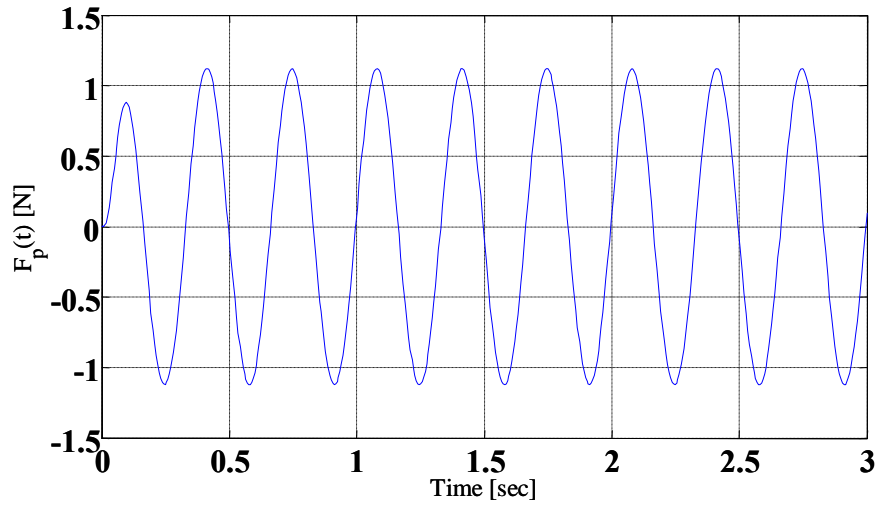


Figure 6.7: Actuator stabilization force of the compensator control system

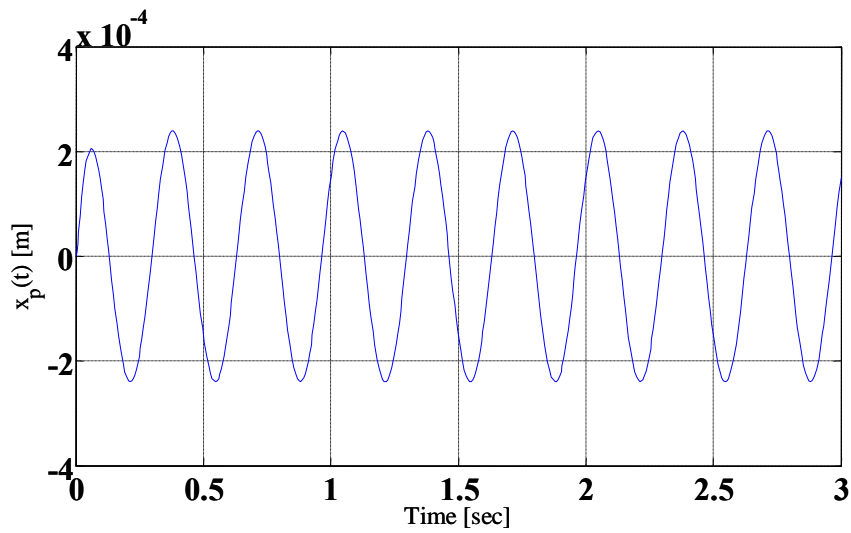


Figure 6.8: Actuator displacement of the compensator control system

6.4 State Feedback

As shown in Figure 6.9 use of a state feedback matrix dramatically decreases the amplitude of $\theta(t)$, the targeting error of the shooter in comparison to the shooter operating an uncontrolled rifle. State feedback moved the closed loop poles of the system closer to the real axis, and further to the left of the $j\omega$ -axis in order to dampen the amplitude of the targeting error and shorten the system's transient response.

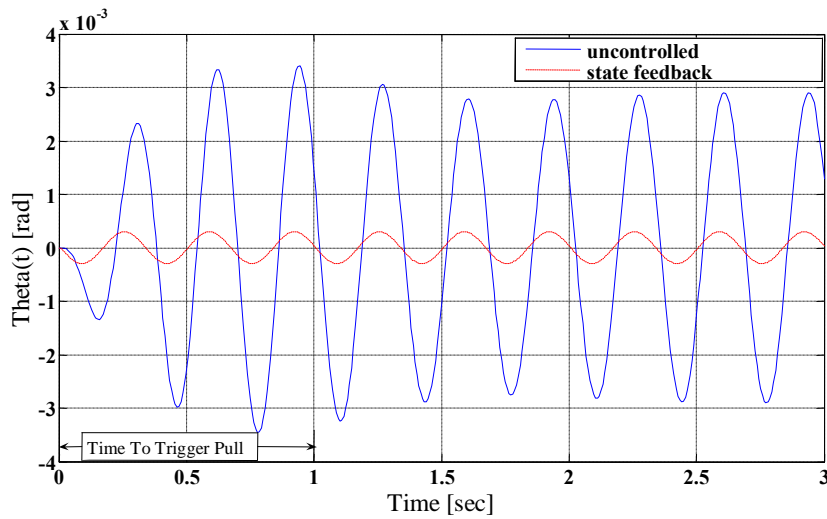


Figure 6.9: Targeting error for uncontrolled system vs. state feedback system

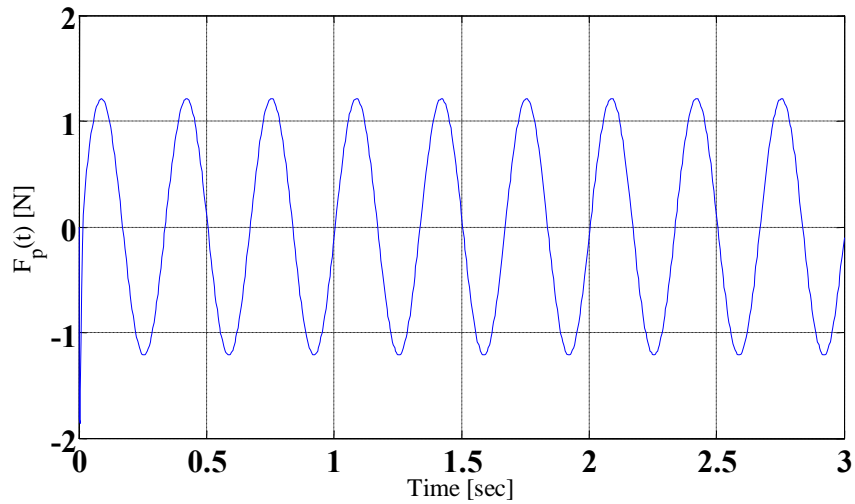


Figure 6.10: Actuator stabilization force of the state feedback control system

The actuator force for the state feedback control system is well under the saturation limit as shown in Figure 6.10. The next parameter of interest is the actuator displacement $x_p(t)$ in Figure 6.11.

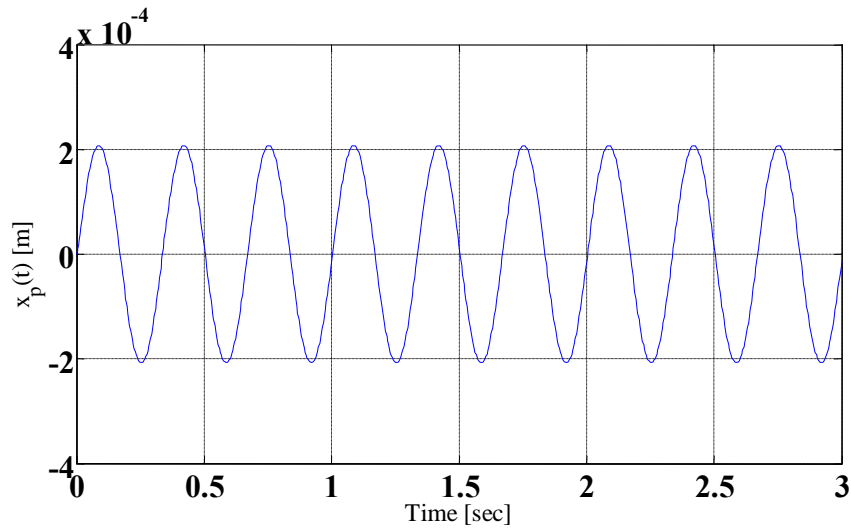


Figure 6.11: Actuator displacement of the compensator control system

For the compensator design, the actuator displacement meets criteria with a maximum displacement of $x_p(t) = 2.2 * 10^{-4} m$

6.5 Observer

In addition to testing to see if the observer design meets the specification criteria like all other control designs, the degree to which the observer is able to estimate the four actual state's values of the system is also analyzed.

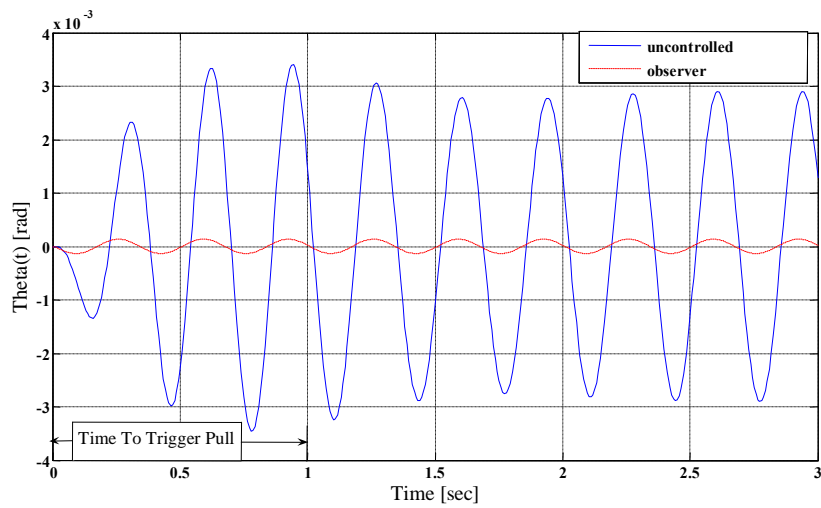


Figure 6.12: Targeting error for uncontrolled system vs. observer system

Figure 6.12 shows the reduction of the targeting error $\theta(t)$ in comparison to the uncontrolled system. The observer does a terrific job at minimizing the human induced disturbances upon the rifle. Figure 6.13 shows the amount of force $F_p(t)$ required by the actuator to produce the results of Figure 6.12.

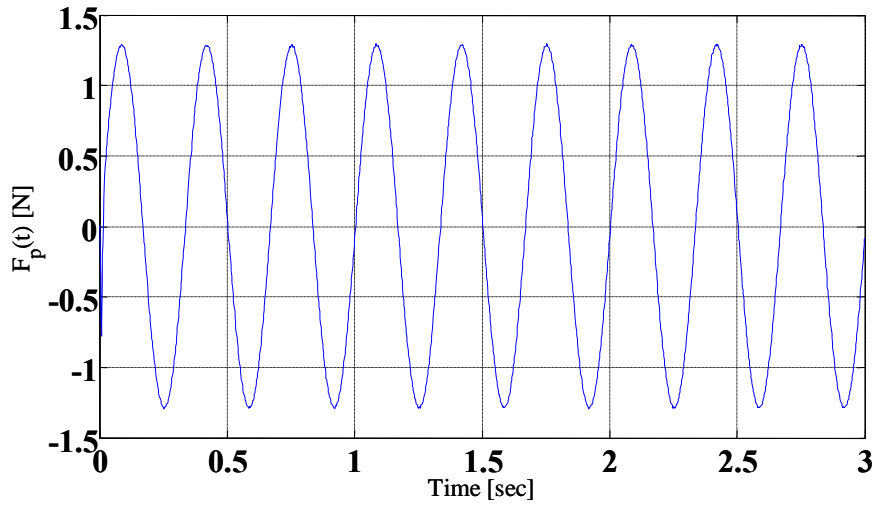


Figure 6.13: Actuator stabilization force of the observer control system

The actuator control does not saturate for the observer control system. It is well within the 8N limit.

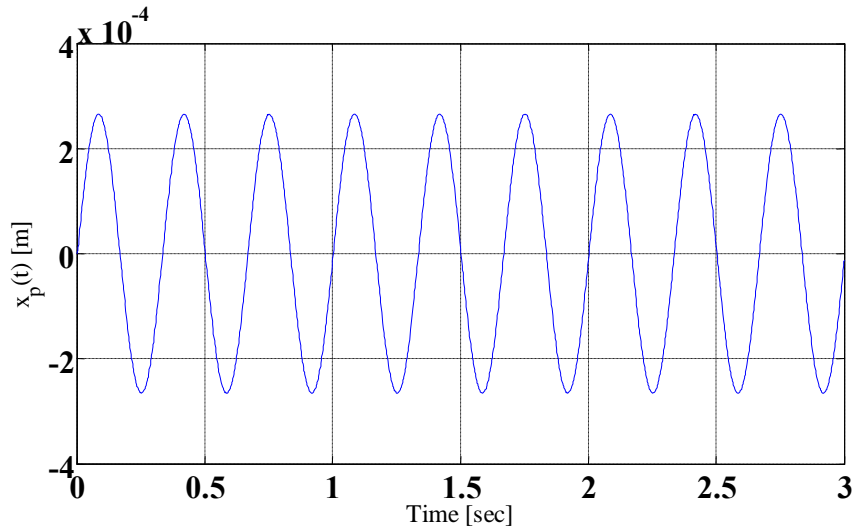


Figure 6.14: Actuator displacement of the observer control system

The actuator displacement for the observer is slightly greater than the displacement of the actuator in the compensator. However the observer system is well within range of the displacement criteria.

Figure 6.15 shows the state variables of the system with respect to their estimates produced by the observer. The true state variable values are represented by a solid blue line, while the estimated state variable values are represented by a dashed red line with “--” point markers.

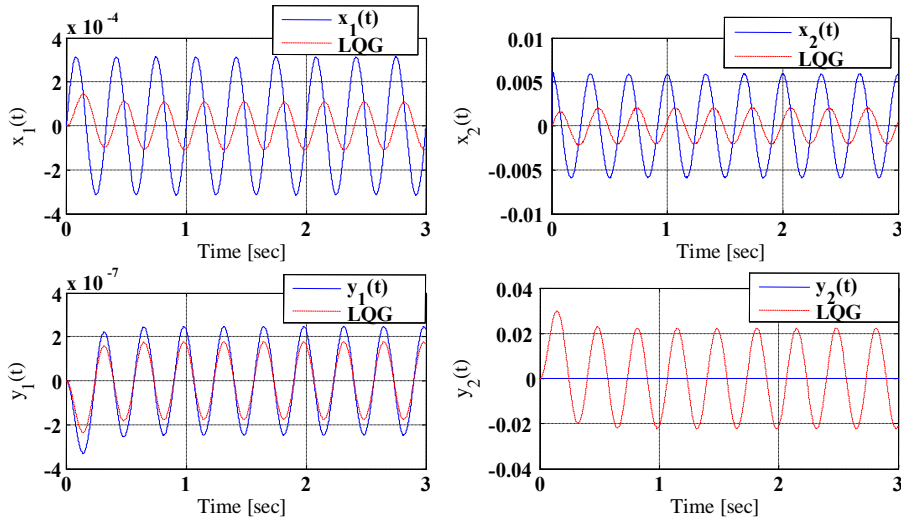


Figure 6.15: Actual state values vs. observer estimated state values

The observer captures precisely the trends for 3 of the 4 system states. Namely, states $x_1(t)$ and $y_1(t)$, which corresponds to $x_p(t)$ and $\theta(t)$, respectively which are used to measure whether the control system's performance meets criteria. These estimated state values are so close to the true state values it looks as if their lines are graphed directly on top of each other in Figure 6.15. In Figure 6.15 the graph of state parameter $x_2(t)$ and its observer estimate shows a lackluster performance of estimating this state's true value by the observer in Figure 6.15.

6.6 LQG

The LQG method produces the lowest targeting error $\theta(t)$ of the barrel in comparison to the other control methods used in the simulations. Figure 6.16 shows the output results of the LQG control method in relation to the uncontrolled system.

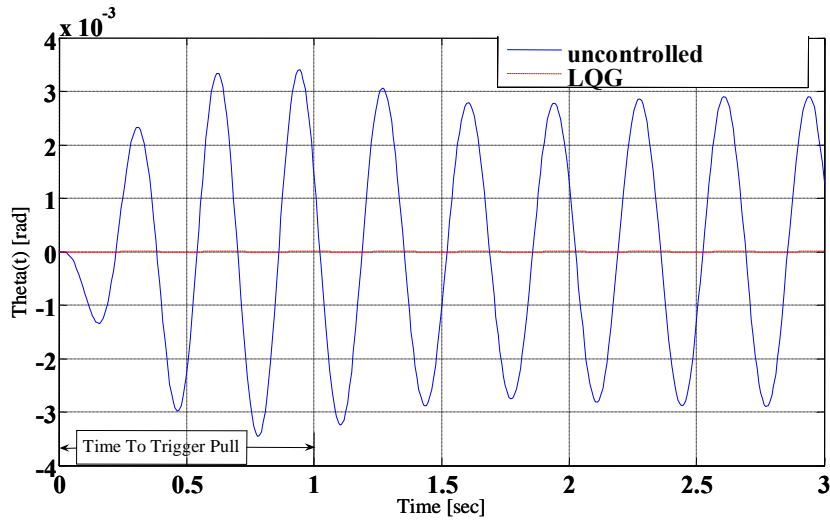


Figure 6.16: Targeting error for uncontrolled system vs. LQG control system

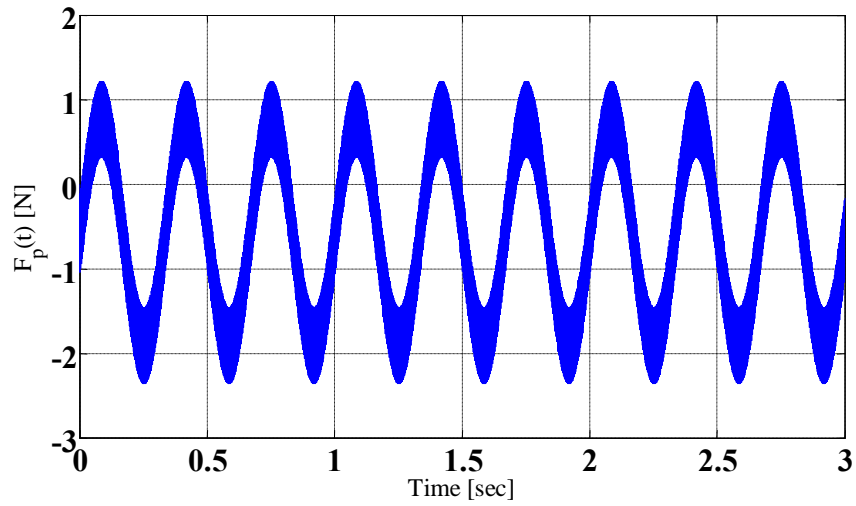


Figure 6.17: Actuator stabilization force of the LQG control system

Figure 6.17 shows that the LQG meets criteria on the amount of force exerted by the actuator to stabilize the system, as a result the actuator does not saturate during the simulation of the LQG control system.

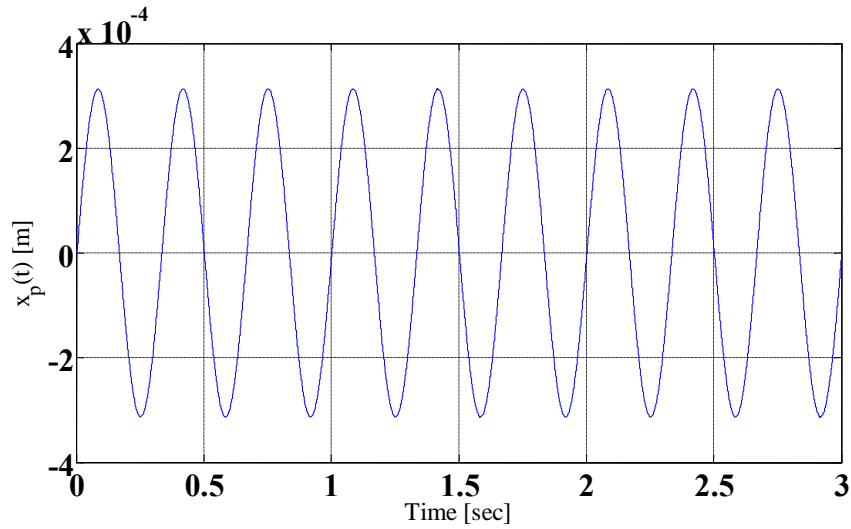


Figure 6.18: Actuator displacement of the LQG control system

The LQG has the largest amplitude for actuator displacement, in comparison to the other control systems. The actuator displacement for the LQG is however within range of the allowed actuator displacement. Even though the LQG method produced the minimum targeting error it did not do as well estimating the state values of the system as did the observer system in the previous section as can be seen in Figure 6.18.

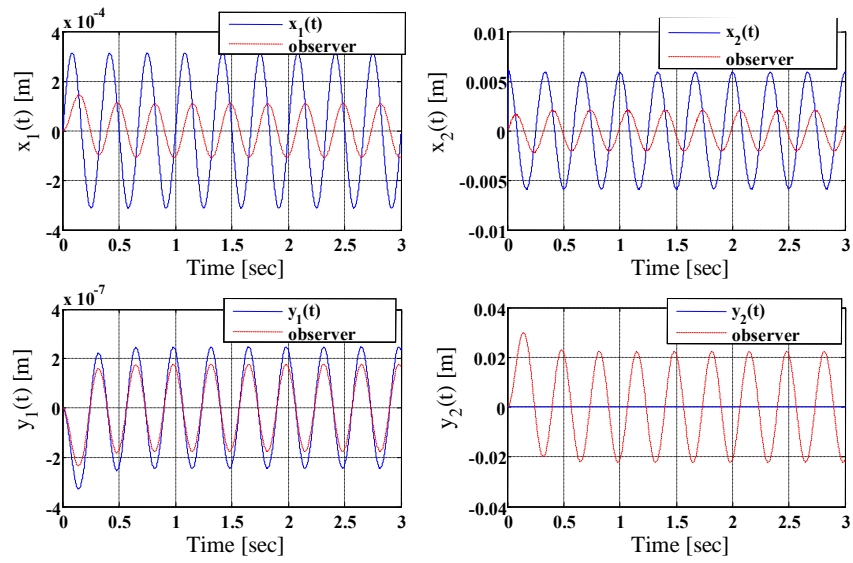


Figure 6.18: Actual state values vs. LQG estimated state values

Chapter 7

Conclusion

In this research we analyzed the equations of motion for the INSTAR system and its actuator design. The information collected was used to develop control design criteria. Upon review of the control design criteria, five controllers were designed. Each controller handles the task of receiving the rifle's targeting error as input and producing a stabilizing input command to the actuator. The design motivation behind the controllers is to produce a command signal to the actuator that reduces barrel jitter that results from human induced disturbances. These controllers include: a unity feedback controller, a compensator controller, a state feedback controller, an observer system controller, and an LQG controller.

Computer simulations were run for all five controllers in a time interval of $0s \leq t \leq 3s$. Within the simulation 3hz disturbance were induced into each controller design. How well each controller measured up to the design criteria determined if the controller reached a level of acceptable performance.

All controllers except for the unity feedback controller, performed at a level of acceptance. The controllers were successful in minimizing the effects of human shooter disturbances in relation to the shooter's targeting error while meeting that actuator's force and displacement criteria.

Even though all controllers except for the unity feedback controller showed acceptable performance, there is no clear cut winner. The controller of choice depends on the operator and designer. The LQG controller produced the minimum targeting in reference to all controllers. However this controller is the most complex out of all system. An LQG system requires a microcontroller which requires its own power source, which may add weight to the weapon as well unwanted noise resulting from the additional amplifiers and power sources. On the other end of the spectrum when it comes to complexity and acceptable performance level is the compensator controller. It is the least complex control system to perform at an acceptable level. It is an analog system which does not need its own power supply, which means no extra noise added to the system from the amplifiers and additional power supplies. The compensator is easier to implement into the INSTAR system than its LQG counterpart. In the middle of the bunch is the observer controller. Its complexity is the in the middle in respect to the compensator and LQG controllers. It is an analog system that doesn't require an external power supply nor a microcontroller. There is no clear cut winning control algorithm in this paper.

7.2 Future Works

Future investigations to be considered in this research due to certain limitations in this paper include applying and developing controllers for the INSTAR system for the M24 sniper rifle. It is standard widely used sniper rifle in the U.S. military. An addition of sensor noise to the observer and LQG designs would provide additional real world criteria for performance level assessment for these controllers. Last but not least built

prototype of each controller tested in real world applications would be very beneficial in the progress of this research for active stabilization systems for small arms weaponry.

References

Clymer, A., 1993, "The Mechanical Analog Computers of Hannibal Ford and William Newell", *IEEE Annals of the History of Computing*, Vol 15, Issue 2.

Brei, D., Luntz, J., and Barnes, B., 2005, "Small Arms gun Barrel Stabilization Using High Energy Density, Rugged, and Low Creep Actuators", June 2005 Specifications Report, University of Michigan, Ann Arbor, MI.

Brei, D., James, V., Lindner, D., Zhu, H., Lavigna, C., 2003, "Development and Demonstration of INSTAR-Inertially Stabilized Rifle", *Proceedings of SPIE Conference*.

Lindner, D., Celano, T., and Ide, E., 1991, "Vibration Suppression Using a Proofmass Actuator Operating in Stroke/Force Saturation", *ASME Journal of Vibration and Acoustics*, Vol 113, pp.423-433.

Mattice, M., and LaVigna, C., 1997, "Innovative Active Control of Gun Barrels Using Smart Materials", *Proceedings of SPIE Conference*, Vol3039, pp630-641.

Pathak, A., Brei, D., Luntz, J., and Lavigna, C., 2006, "A Dynamic Model for Generating Actuator Specifications for Small Arms Barrel Active Stabilization", University of Michigan & Techno-Sciences, Inc., Ann Arbor, MI & Lanham, MD.

Siddle, Bruce. "Psychological Effects Of Combat" 2000.

http://www.killology.com/art_psych_combat.htm